TAMPEREEN TEKNILLINEN YLIOPISTO
TAMPERE UNIVERSITY OF TECHNOLOGY
Julkaisu 850 • Publication 850

Anne Kotiaho

Gold Nanoparticle-Chromophore Systems

Assembly and Photophysical Interactions

Tampere 2009

Tampereen teknillinen yliopisto. Julkaisu 850
Tampere University of Technology. Publication 850

Anne Kotiaho

Gold Nanoparticle-Chromophore Systems

Assembly and Photophysical Interactions

Thesis for the degree of Doctor of Technology to be presented with due permission for public examination and criticism in Festia Building, Auditorium Pieni Sali 1, at Tampere University of Technology, on the 27th of November 2009, at 12 noon.

Tampereen teknillinen yliopisto - Tampere University of Technology
Tampere 2009

ISBN 978-952-15-2266-6 (printed)
ISBN 978-952-15-2278-9 (PDF)
ISSN 1459-2045

Abstract

Thin films of gold nanoparticles and photoactive organic molecules were prepared and studied with photoelectrical, spectroscopic and microscopic methods. Photoinduced electron transfer takes place from a poly(hexylthiophene) layer to the gold nanoparticle layer, and in the case of a porphyrin or a fullerene layer, the gold nanoparticles donate electrons to these chromophores. The photoelectrical measurements indicate that the particles can function either as electron acceptors or donors to the photoexcited chromophores. The highest photoelectrical signal was observed for films combining gold nanoparticles and porphyrin-fullerene dyads. Porphyrin-fullerene dyads are known to undergo intramolecular photoinduced charge transfer via an exciplex intermediate state. A gold nanoparticle layer enhances charge transfer of the dyad, when placed near the porphyrin moieties of the dyads. In addition, fluorescence measurements indicated that the gold nanoparticle layer affects the relaxation of the exciplex state of the dyad. The photoelectrical measurements demonstrated charge transfer in the films of porphyrins and gold nanoparticles, but energy transfer was considered to be possible as well. Time-resolved spectroscopic measurements showed that most, more than 80%, of the photoexcited porphyrins decay by energy transfer to the gold nanoparticles, whereas charge transfer is a minor relaxation route.

Porphyrin- and phthalocyanine-functionalized gold nanoparticles were prepared using a ligand exchange method and characterized with steady-state and time-resolved spectroscopic techniques. The photoexcited porphyrins transfer energy to the gold cores very rapidly, in few picoseconds. The packing of the porphyrins on the gold nanoparticle surface and their fluorescence lifetimes are dependent on position of the linkers on the porphyrin core. Time-resolved absorption measurements were used to study the fast photoinduced processes of the phthalocyanine-functionalized gold nanoparticles. The selective excitation of the gold cores leads to energy transfer to the phthalocyanines. Photoexcitation of the phthalocyanines results in energy and electron transfers to the gold cores.

As a conclusion, the photoinduced charge and energy transfer processes of the gold nanoparticle-chromophore systems studied are dependent on the choice of the chromophore and on the design of the system.

Preface

I thank my supervisor Prof. Helge Lemmetyinen for the possibility to join the excellent photochemistry research group and for having his office door open whenever any bigger problems occurred during my work. My co-supervisor Dr. Riikka Lahtinen I thank for being extremely supportive in all aspects regarding work and other things as well. I thank Riikka for allowing me great freedom in carrying out this work and having optimistic advices every time I got stuck with the work.

To Prof. Nikolai Tkachenko I am thankful for all the explanations on physics and for the helpful comments on my manuscripts. I thank Dr. Alexander Efimov for introducing me to the world of synthetic chemistry. I appreciate Dr. Vladimir Chukharev's help on practical matters in the lab. I thank Heli Lehtivuori for discussions on spectroscopy and other topics. Special thanks on laboratory work well done go to Essi Sariola and Hanna-Kaisa Metsberg.

I am grateful to all the people of the chemistry lab for the nice working atmosphere. Especially I thank my wonderful roommate Dr. Marja Niemi for sharing both the annoying and cheerful moments during this time and also my long term co-worker Dr. Kimmo Kaunisto.

I thank my family for their support. My brother Tommi I thank for encouragement and pastime. My deepest gratitude I owe to my beloved husband Kalle for standing by me and for all the joy we have shared over the years.

This work was carried out at the Department of Chemistry and Bioengineering in Tampere University of Technology during years 2005-2009. The Academy of Finland is gratefully acknowledged for funding (No. 107182).

Tampere, November 2009

Anne Kotiaho

Contents

List of publications

The Thesis is based on the work contained in the following publications, which are hereafter referred to by their Roman numerals:

I **Gold nanoparticle enhanced charge transfer in thin film assemblies of porphyrin-fullerene dyads**

Anne Kotiaho, Riikka Lahtinen, Nikolai V. Tkachenko, Alexander Efimov, Aiko Kira, Hiroshi Imahori and Helge Lemmetyinen, *Langmuir* **2007**, *23*, 13117-13125.

II **Photoinduced energy and charge transfer in layered porphyrin-gold nanoparticle thin films**

Anne Kotiaho, Riikka Lahtinen, Heli Lehtivuori, Nikolai V. Tkachenko and Helge Lemmetyinen, *J. Phys. Chem. C* **2008**, *112*, 10316-10322.

III **Effect of gold nanoparticles on intramolecular exciplex emission in organized porphyrin-fullerene dyad films**

Anne Kotiaho, Riikka Lahtinen, Hanna-Kaisa Latvala, Alexander Efimov, Nikolai V. Tkachenko and Helge Lemmetyinen, *Chem. Phys. Lett.* **2009**, *471*, 269-275.

IV **Synthesis and time-resolved fluorescence study of porphyrin-functionalized gold nanoparticles**

Anne Kotiaho, Riikka Lahtinen, Alexander Efimov, Heli Lehtivuori, Nikolai V. Tkachenko, Tomi Kanerva and Helge Lemmetyinen, *submitted for publication.*

V **Photoinduced charge and energy transfer in phthalocyanine-functionalized gold nanoparticles**

Anne Kotiaho, Riikka Lahtinen, Alexander Efimov, Hanna-Kaisa Metsberg, Essi Sariola, Heli Lehtivuori, Nikolai V. Tkachenko and Helge Lemmetyinen, *submitted for publication.*

Author's contribution

Anne Kotiaho has either planned or carried out almost all the experimental work and data analysis and written all the publications listed above.

Abbreviations and symbols

AFM	atomic force microscopy
C	capacitance
C_{60}	buckminsterfullerene
CCD	charge coupled device
cis-Por	2-[3-[5-[3-[2-(3-acetylsulfanylpropanoyloxy)ethoxy]phenyl]-15,20-bis(3,5-di-*tert*-butylphenyl)porphyrin-10-yl]phenoxy]ethyl 3-acetylsulfanylpropanoate
cis-Por-AuNP	gold nanoparticles functionalized with *cis*-Por molecules
C_6SAu	hexanethiol-protected gold nanoparticle
C_8SAu	octanethiol-protected gold nanoparticle
d, D	distance
d_0	critical distance of energy transfer
DAF	3'-cyclopropa[1,9][5,6]fullerene-C60-3',3'-dicarboxylic acid
DAS	decay associated spectrum
DHD6ee	61,62-diethyl [10,20-(3-(2-hydroxyethoxy)-phenyl)porphyrin-5,15-diylbis(1-phenyl-3-oxy)diethylene] 1,9:49,59-bismethano[60]fullerene-61,61,62,62-tetracarboxylate
e	elementary charge
F	fluorescence intensity
FLM	fluorescence lifetime microscopy
FRET	Förster resonance energy transfer
g	amplifying factor
h	Planck constant
HOMO	highest occupied molecular orbital
I_0	saturation excitation energy density
I_{exc}	excitation energy density

ITO	indium tin oxide
LB	Langmuir-Blodgett
LS	Langmuir-Schäfer
LUMO	lowest unoccupied molecular orbital
MCA	multichannel analyzer
n	parameter for molecular organization, surface density
NIR	near-infrared
ODA	octadecyl amine
Pc	1,4-di[(3-acetylsulfonylpropanoate)propyloxy]-9(10),16(17),23(24)-tri[*tert*-butyl]-phthalocyanine
Pc-AuNP	gold nanoparticles functionalized with Pc molecules
PF	porphyrin-fullerene dyad
PHT	poly(3-hexylthiophene-2,5-diyl)
R_{in}	input resistance
S_{el}	electrode area
SET	surface energy transfer
SHG	second harmonic generator
TAC	time-to-amplitude converter
TBD6a	61,62-[10,20-(3,5-di-*tert*-butylphenyl)porphyrin-5.15-diylbis(1-phenyl-3-oxy)diethylene] 1,9:49,59-bismethano[60]fullerene-61,61,62,62-tetracarboxylate
TBP	5,10,15,20-tetrakis(3,5-di-*tert*-butylphenyl)porphyrin
TCSPC	time-correlated single photon counting
TEM	transmission electron microscopy
TOABr	tetraoctylammonium bromide
TOABr-AuNP	tetraoctylammonium bromide-protected gold nanoparticles
trans-Por	2-[3-[15-[3-[2-(3-acetylsulfanylpropanoyloxy)ethoxy]phenyl]-10,20-bis(3,5-di-*tert*-butylphenyl)porphyrin-5-yl]phenoxy]ethyl 3-acetylsulfanylpropanoate

trans-Por-AuNP	gold nanoparticles functionalized with *trans*-Por molecules
TRMDC	time-resolved Maxwell displacement charge
U_0	saturation photovoltage amplitude
U_{bias}	external voltage
U_{out}	photovoltage amplitude
UV	ultraviolet
β	stretching parameter
φ	quantum efficiency of charge transfer
ν	frequency
σ	absorption cross section
τ	lifetime

1 Introduction

Dream of alchemists was to transform less-valuable materials into precious gold. A surprise for them would be that modern science has come up with a form of gold that might turn out to be even more valuable than shiny gold, that is, gold nanoparticles.

Gold colloids, which contain fine pieces of gold dispersed in a liquid, have been known for centuries for their magnificent colours and used in staining glass. The scientific approach towards gold colloids dates back to 1850's, and to Michael Faraday, who discovered the relation between the colour and the small size of the colloidal particles.[1] Nanoparticles as a term refer to particles with size from few to several hundreds of nanometers (10^{-9} m). The intriguing properties of nanoparticles rise from them being bigger than molecules, but too small to have properties of bulk material.

Since 1990's, the number of publications related to gold colloids and nanoparticles has increased rapidly.[2] Research field focused on gold nanoparticles is expanding and evolving with 3M principle: make, measure and model.[3] These three factors lead to continuous progress within the research field, where discoveries and development[4] in controlled preparation, observed phenomena and theoretical explanations will combine into successful applications.

There are two principal strategies for preparing metal nanostructures: top-down and bottom-up approaches. The top-down methods, such as laser ablation[5] and lithography[6], remove portions of material to create smaller structures. The bottom-up methods, for example chemical synthesis and self-assembly, combine atoms and molecules into nanostructures. The most popular metals for chemically prepared nanoparticles have been gold and silver, with gold nanoparticles having the advantage of being chemically stable.

Metal nanoparticles have size-dependent optical and electronic properties. An important feature of metal nanoparticles is the localized surface plasmon band resonance[6], which is seen as high extinction coefficients of metal nanoparticles. Smaller metal nanoparticles absorb light intensively, whereas scattering of light becomes an important factor for bigger nanoparticles. The surface plasmon band resonance causes enhancement of electromagnetic field near the metal nanoparticles. Applications utilizing the surface plasmon resonances of metal nanoparticles include imaging, sensing, medicine, photonics and optics.[7-8] The electronic properties of metal

nanoparticles include charge storage and conductivity,[9] which have been utilized for example in memory devices[10-12] and molecular switches[13]. One significant feature of gold nanoparticles is their catalytic activity[2,14-15], which is an ability that bulk gold is lacking.

The wide application range of gold nanoparticles themselves can be broadened by combining them with organic molecules having specific chemical functions, for example photoactivity or recognition properties. Functionalization of gold nanoparticles offers a route to modify properties of both the gold core and the functional molecules, leading to formation of hybrid materials with new properties. Functionalized gold nanoparticles have at least sensing[16] and biological[17-18] applications and they serve as building blocks for materials with nanoscale organization[19-21].

Visible light is one form of electromagnetic radiation and it can initiate chemical reactions. The most important of light-initiated processes is photosynthesis, where plants use energy from sunlight to produce sugar and oxygen from carbon dioxide and water. Green plants have in them a light-absorbing compound, chlorophyll. Synthetic chemists have made their artificial analogues of chlorophyll, for example porphyrin and phthalocyanine. Porphyrin and phthalocyanine absorb light effectively and can participate in photoinduced charge and energy transfer reactions.[22] Photoinduced charge separation can be effectively reached in porphyrin-fullerene donor-acceptor molecules[23], where the photoexcited porphyrin transfers an electron to the fullerene. Efficient formation of the charge-separated state with a long lifetime in the porphyrin-fullerene dyad can be utilized in photovoltaic applications, where energy from light is converted into electrical potential.[24]

The combination of photoactive molecules, chromophores, with gold nanoparticles into hybrid systems can lead to several interaction mechanisms. Typical photoinduced processes of the hybrid systems are charge or energy transfer[25] and fluorescence enhancement[26-27]. Photoinduced charge and energy transfer from the chromophores to the particles result in quenching of the chromophore fluorescence. Charge and energy transfer are favoured by a smaller core size (< 30 nm) of the gold nanoparticles and a short distance (< 10 nm) between the chromophores and the particles. Fluorescence enhancement, on the other hand, is supported by bigger gold nanoparticles at longer distances from the chromophores.

In the present study, two strategies to combine chromophores and gold nanoparticles were used: deposition as adjacent thin films and covalent attachment of the chromophores on the gold nanoparticle surfaces. The chromophores chosen for detailed studies of films were porphyrin and

porphyrin-fullerene dyads. Porphyrin and phthalocyanine molecules were utilized in the covalently attached assemblies. The effect of photoexcitation on the hybrid systems was studied with steady-state and time-resolved spectroscopic measurements, and in case of films, also with time-resolved photoelectrical measurements. The energy and charge transfer processes were observed both in films and in covalently linked assemblies, indicating applicability of both preparation strategies. The gold nanoparticles show indeed promise for building block preparation, because they can participate in energy and electron transfer reactions, which are controlled by the selection of the accompanying chromophore and by the organization of the gold nanoparticle-chromophore structure.

2 Background

Absorption and emission are important properties for the use of gold nanoparticles in photoactive devices. The electronic properties of gold nanoparticles give rise to their usability in charge transfer systems. Understanding the principal properties of these particles helps in getting a grasp of the properties of chromophore-gold nanoparticle systems. Most of the processes considering interaction of chromophores with gold nanoparticles are well characterized, but the fine details of the mechanisms are not fully understood. In the next paragraphs the preparation and properties of gold nanoparticles and their interaction with chromophores are discussed from the literature point of view and the chromophores used in this work are introduced in more detail.

2.1 Preparation and properties of gold nanoparticles

The ease and controllability of metal nanoparticle preparation has been greatly enhanced due to discovery and improvement of several synthetic methods. A variety of metals can be used for chemical preparation of nanoparticles, including gold, silver, platinum, copper, cobalt, palladium, nickel and iron.[28] The most popular metal has been gold due to the stability of the nanoparticles. Silver has also been widely used, despite its tendency for oxidation. With different synthetic procedures[29-33], it is possible to produce spherical gold nanoparticles with desired solubility and size. Furthermore, gold nanoparticles can be prepared in rod, prism, cubic and branched shapes.[34]

Widely used methods for preparation of spherical gold nanoparticles are citrate reduction introduced by Turkevitch[35] *et al*. in 1951 and a two-phase method using thiols suggested by Brust[36] *et al*. in 1994. In both of these reactions, the particles are formed by reduction of gold precursors and stabilized against aggregation with organic molecules. The Turkevitch method produces water soluble particles stabilized electrostatically by citrate molecules. The particles prepared with the Brust method are stabilized by covalently bound thiols and are called monolayer-protected clusters[37]. The monolayer-protected clusters have proven to be versatile materials, because the thiol monolayer acts as efficient stabilizer that endures chemical modification. Other stabilizers for gold nanoparticles besides thiols and citrate include, for example, amines, phosphines, polymers and dendrimers.[15] The Brust reaction without addition of thiols produces particles stabilized by surfactant molecules.[38]

Though routes to metal nanoparticles have been known for some time, the detailed optical and electrochemical studies have been possible only after the synthetic methods for producing particles monodisperse in size were developed. Size distribution of gold nanoparticles can be controlled by the choice of reaction conditions[39-41] or post-synthetic treatments. For example, heat treatment after the initial formation of the particles can be used to control both the size and dispersity of the particles.[42-44] Purification and separation according to size can be carried out using fractional precipitation[45] or size exclusion chromatography[46].

2.1.1 Optical properties

Gold nanoparticle solutions have an intense red colour, which changes to brown when the particles are small (~2 nm) and to violet in the case of big nanoparticles. The red colour originates from absorption or scattering of light around 520 nm by localized surface plasmons. Because the particles absorb strongly green light, they appear red. Surface plasmon band is a characteristic, size-dependent property of metal nanoparticles. The surface plasmon band arises from collective oscillations of conduction band electrons. The conduction band electrons are considered to be free electrons, which can follow oscillations of an electric field. The electric field of incident light couples with the conduction band electrons and polarizes them relative to the heavy centre of the nanoparticle.[47] This leads to a charge difference between the opposite surfaces of the nanoparticle, which then acts as a restoring force and causes dipolar oscillation of the electrons.[47] Valence band electrons, on the contrary to conduction band, are considered as bound electrons, but they can be optically excited as well. Upon excitation, the valence band electron is promoted to a state of higher energy, that is, to conduction band. Steady rise of gold nanoparticle absorption at blue wavelengths is due to these interband transitions, whose absorption onset is around 520 nm[48].

Interaction of electromagnetic field with small, metallic spheres was first theoretically described by Mie, by solving Maxwell's equations, and his theory still remains well applicable with some improvements[49]. The Mie theory predicts the dependence of the plasmon band position and intensity on the size and surroundings of the metal sphere. According to Mie theory, smaller (< 40 nm) gold spheres mainly absorb light, whereas bigger gold spheres are efficient light scatterers.[50] As the size of the particle increases, extinction (absorption + scattering) coefficient increases and the plasmon band shifts to red.[50] Extinction coefficients of gold nanoparticles of core diameters 4-40 nm are 10^6-10^9 M^{-1} cm^{-1}.[51] The extinction coefficients of gold nanoparticles are orders of magnitude higher than those of traditional organic dyes.

The surface plasmon band is not present for small gold nanoparticles (< 2 nm), but there is an onset of absorption at the energy corresponding to interband transition edge.[45,52] Absorption spectrum of small particles has a step-like structure, which indicates discrete energy levels.[45,52] Behaviour of gold clusters of core diameter < 1 nm turns from metallic into non-metallic and a clear band gap is observed.[53] Thus, 1 nm diameter can be considered as a limit for quantization of energy levels.

Excitation of gold nanoparticles with short laser pulses increases energy, i.e. temperature, of the electrons. In order to return to their initial state, the electrons have to lose the gained energy either as heat (phonons) via collisions or as light (photons) by emission. Relaxation of the excited gold nanoparticles without emission of photons proceeds through three steps. First, the high temperature electrons distribute their energy among all the electrons by electron-electron scattering in less than a picosecond.[54-55] Second, energy is transferred from electrons to whole of the particle via electron-phonon scattering during few picoseconds.[48,56] The transfer of heat from the particle to the surrounding medium via phonon-phonon scattering is the third step, which proceeds in hundreds of picoseconds.[48,56] The relaxation time constants are dependent on the excitation energy[57-58], excitation wavelength[54] and surrounding medium[59].

The alternative pathway for relaxation of excited electrons in gold nanoparticles is photon emission. Fluorescence has been observed for small, molecular and for bigger, metallic gold nanoparticles, but the emission mechanisms for these two size regimes are different. Small particles have a distinct HOMO-LUMO gap, and a photon is released as a result of recombination of the excited electron with a hole,[60-63] just as in simple fluorescent molecules the photoexcited electron returns back to ground state via photon emission. The protecting ligand has a significant effect on the luminescence of small particles (< 2 nm).[64-65] Very small gold nanoclusters can yield high emission, because as the energy levels become more separated, the non-radiative decay is depreciated.[66] The factors limiting the fluorescence quantum yield of gold nanoparticles can be transformation of energy to heat through ligand or solvent[63] or insufficient purification[61]. The fluorescence of big gold nanoparticles is quite a controversial issue[67] with different mechanisms, such as recombination of an electron and a hole[68] and plasmon emission [69-70], proposed.

2.1.2 Electronic properties

Electronic and optical properties of gold nanoparticles are size-dependent. Thiol-protected gold nanoparticles have a metallic core surrounded by an insulating monolayer. Ions of a conducting electrolyte surround the thiol-protected gold nanoparticles in electrochemical measurements, where it is possible to charge the gold cores. Very small particles (~1 nm) show redox character, similar to electrochemical charging of electroactive molecules.[71] A band gap similar to that obtained from the absorption spectrum is observed in electrochemical measurements.[71] The electrochemical behaviour of particles that are large enough to be metallic, but have high enough capacitance (core diameter < 4 nm[72]) for the single electron charging to be visible at room temperature can be described as quantized double layer charging.[73] Up to 15 redox states have been observed for 2 nm particles with a narrow size distribution.[74] Gold nanoparticles can be used to store charge[75], similarly to a capacitor in electrical circuits. It has been assumed that the charge state of thiol-protected gold nanoparticles prepared via the Brust reaction is -1 due to the strong reducing agent used in the reaction.[74]

The electrochemical measurements of thiol-protected gold nanoparticles show charging of the gold cores and they can show conductivity in solid form. The conductivity of solid gold nanoparticles is controlled by two factors: the number of charge carriers and the distance between the gold cores. Charge carriers in films of gold nanoparticles are created by a disproportionation reaction, where two neutral cores produce one negatively and one positively charged core.[76] Alternatively, gold cores can be charged electrochemically in a solution, then dried and deposited as a film, to increase the number of charge carriers.[76] Disproportionation is a thermal reaction, and higher temperatures produce a large number of charge carriers. The charge carriers can hop to a neutral core, giving rise to an increase in conductivity.[77] For transfer from one core to the next one, electrons (or holes) have to tunnel through the dielectric thiol-layer between the gold cores.[77] Tunneling is more efficient at short distances. Therefore, the conductivity of solid thiol-protected gold nanoparticles increases with decreasing length of the protecting thiol[77] or in the case of Langmuir films, mechanical compression of gold cores closer to each other increases conductivity of the film[78-79].

2.2 Porphyrinoids, fullerenes and porphyrin-fullerene dyads

Porphine (Figure 2.1A) is a planar, conjugated macrocycle, to which chlorophyll of green leaves and hemoglobin of human blood have structural similarities. Substituted porphines are

called porphyrins, and together with other porphine derivatives such as phthalocyanine (Figure 2.1B) they form a class of compounds called porphyrinoids.

Synthetic methods for production of porphyrins and phthalocyanines have been available from the beginning of the 20th century, allowing detailed characterization and development of a wide range of applications to date. The intense colour of porphyrins (red) and phthalocyanines (blue-green) arise from the highly conjugated structure. Porphyrins absorb light intensively around 400 nm (Soret-band) due to electronic transition from ground state to the second excited singlet state. Molar absorption coefficient of porphyrin at the Soret-band is high, > 200 000 M^{-1} cm^{-1}. In addition to the Soret-band, porphyrins have weaker Q-bands at longer wavelengths. The Q-band absorbance corresponds to electronic transitions to the first excited singlet state. Relaxation of the first excited singlet state of porphyrins is relatively slow and thus the excited state has time to react with other molecules, for example via energy or electron transfer. Phthalocyanines absorb light on a wider wavelength range compared to porphyrins due to stronger Q-bands. Porphyrins and phthalocyanines can accommodate a metal atom inside their ring structure instead of the hydrogen atoms shown in Figure 2.1A and B. The central metal atom affects the properties of porphyrinoids together with the peripheral groups. Despite the structural similarities of porphyrins and phthalocyanines, their redox properties are different.[22,80-82]

The history of fullerene (C_{60}, Figure2.1C) does not date as far as that of porphyrinoids, since it was discovered in the middle 80's[83]. Fullerenes in general consist of twelve 5-membered rings and an unspecified number of 6-membered rings that together form an enclosed structure.[84] Buckminsterfullerene, C_{60}, is a ball-shaped molecule composed of 60 carbon atoms. Fullerene is one of the crystalline forms of carbon, in addition to graphene and diamond. Fullerene is a good electron acceptor: up to 6 electrons can be accommodated on a fullerene molecule.[85] Fullerene shows also photochemical activity due to strong absorption in the UV-range.[84]

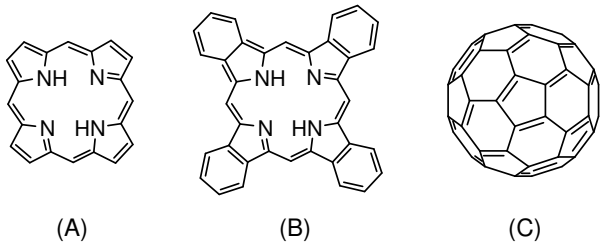

Figure 2.1. Chemical structures of (A) porphine, (B) phthalocyanine and (C) fullerene (C_{60}).

Porphyrin and fullerene make a good pair for photoinduced electron transfer. Photoinduced charge transfer between porphyrin and fullerene can be optimized in donor-acceptor molecules, called dyads, by forcing the molecules close to each other using a linker. Porphyrin-fullerene dyads undergo fast and efficient intramolecular charge transfer in polar solvents.[86-90] Importantly, the charge recombination is slower than the charge separation, which results in relatively long-living charge separated states.[86-90] Porphyrin-fullerene dyads have been self-assembled for photocurrent generation.[91-92] The earliest dyads had one linker, which allows movement of the fullerene and porphyrin relative to each other. Charge separation efficiency is improved, when two linkers are used.[93-95]

2.3 Gold nanoparticle-chromophore systems

Chromophore as a term points usually to the part of a molecule responsible for the colour of the compound. Here, a chromophore denotes light-absorbing molecules in general. Gold nanoparticle-chromophore systems are discussed mostly in terms of functionalized gold nanoparticles. Film assemblies of chromophores and gold nanoparticles are not discussed here in detail, except for the combinations of porphyrin, phthalocyanine and fullerene with gold nanoparticles. Metal nanoparticles in films can increase performance of solid organic photovoltaic devices, where they function as light absorbers[96-99], recombination centres[100-101], buffer layers[102-103] or improvers of conductivity[104].

2.3.1 Preparation of gold nanoparticle-chromophore assemblies

Chromophore-functionalized gold nanoparticles can have the chromophore attached either by electrostatic[105-107] or covalent binding[108-112]. The chromophores serve also as a protecting layer in the functionalized particles. The electrostatic assemblies are relatively easy to prepare by mixing gold nanoparticles protected with charged ligands with the oppositely charged chromophores. The downside of the electrostatic assemblies is that they cannot be dried from the solution. The gold nanoparticles protected with covalently bound chromophores are in principle stable enough to be extracted from solution and even processed into films.

There are several strategies to prepare covalently linked chromophore-gold nanoparticle assemblies. The chromophore-functionalized particles can be formed just in the same way as simple thiol-protected particles if a chromophore with a thiol group is used. The compatibility of the reducing agent and the chromophore has to be taken into account: the reduction step should

not destroy the photoactive thiol.[113] An alternative route to functionalized gold nanoparticles is ligand exchange[114]. Thiol exchange is in principle very simple: by placing thiol-protected gold nanoparticles in a thiol solution, part of the attached thiols are exchanged by thiols in the solution. The limitation of the thiol exchange method is the requirement of similar polarity and size of the attached and the incoming ligands in order to achieve an efficient exchange[115-116]. Protecting thiols of the gold nanoparticles can be tailored to have functional groups such as carbonyl, carboxyl or amine, which undergo, for example, addition reactions and amide or ester coupling reactions with functional groups in the chromophores.[117-118] The reactive functional groups of the protecting monolayer of the gold nanoparticles allow attachment of chromophores using routine chemical reactions.

Gold nanoparticle films can be prepared on solid substrates for example, by solvent evaporation (drop-casting), by Langmuir film methods[119] or by layer-by-layer[120] deposition. In principle, all of these techniques can be applied on the assembly of chromophores together with gold nanoparticles.

2.3.2 Photophysical interactions in gold nanoparticle-chromophore systems

Fluorescence of chromophores is usually efficiently quenched when they are self-assembled on bulk gold surfaces but in spite of this, chromophore layers self-assembled on gold films have applications, for example, in sensors, photocurrent generation and catalysis.[121] The vicinity of a metal nanoparticle to a photoexcited chromophore can affect the relaxation of the chromophore at least via three processes: 1) charge transfer, 2) energy transfer and 3) modification of the radiative rate of the chromophore. Energy and charge transfer are both non-radiative relaxation routes that become available for the chromophore when combined with gold nanoparticles.

Pyrene-functionalized gold nanoparticles were the first gold nanoparticle systems for which photoinduced electron transfer was observed from optical measurements.[108] Electron transfer takes place from photoexcited pyrenes to 2-3 nm gold nanoparticles but this requires a small distance between the nanoparticle and the pyrene molecules.[122] Chlorophyll molecules assembled electrostatically on 8 nm diameter gold nanoparticles transfer electrons to the particles after photoexcitation.[107] In all these systems, close proximity of chromophores and gold nanoparticle is a prerequisite for electron transfer to take place.

Reports on photoinduced energy transfer in gold nanoparticle-chromophore systems outnumber those on charge transfer. Energy transfer has been observed in several gold

nanoparticle-chromophore systems, where particle size and distance between the chromophores and the particles varies over a wide range. Different types of fluorescent compounds, including small dyes[109-112], conjugated polymers[106], semiconductor quantum dots[123] and large molecules such as porphyrin[124] and fullerene[125] show quenching of fluorescence on gold nanoparticle surfaces due to energy transfer. The main direction of energy transfer is from the excited chromophore to the gold nanoparticles, but in principle, energy transfer can also occur from excited gold nanoparticles to close-by chromophores.

Energy transfer can take place via two principal mechanisms,[126] called Dexter and Förster energy transfers. The Dexter energy transfer is a short range (< 1 nm) electron exchange mechanism. The Dexter mechanism requires overlap of molecular orbitals of donor and acceptor. The Förster type energy transfer can take place over longer distances, up to 10 nm, and it is based on Coulombic dipole-dipole interactions. The rate of Förster energy transfer is inversely proportional to distance, $rate \propto (d_0/d)^n$. The exponent n is determined by the dimensionality of the system: energy transfer between two isolated molecules (point dipoles) results in $n = 6$, while energy transfer between a molecule and a surface gives $n = 4$ and for energy transfer between two planes, $n = 2$.[127-128] d_0 is called the critical distance or the Förster radius, which depends on the spectral overlap of donor fluorescence and acceptor absorption spectra, the relative orientation of the molecular dipoles and on fluorescence quantum yield of the donor.

Förster resonance energy transfer (FRET) between two dipoles can be applied in principle to gold nanoparticle-chromophore energy transfer. Experiments have shown, however, that energy transfer in gold nanoparticle containing systems can range up to 20 nm,[129] which is beyond the Förster range. A better way is thus to treat the chromophore as a dipole and the gold nanoparticle as a surface, which leads to a d^{-4} dependence of energy transfer rate. This mechanism is called surface energy transfer (SET) and has been applied to several chromophore-gold nanoparticle systems.[129-130] This has clearly some analogy with FRET, but the critical distance is determined from different physical parameters: the donor quantum yield, the frequency of donor electronic transition, Fermi frequency and wave vector of the metal.[129] In SET, by contrast with FRET, the electromagnetic field of the donor dipole interacts with the conduction electrons of the metal and therefore resonant electronic transition is not needed.[129]

The total decay rate of a photoexcited chromophore is the sum of non-radiative and radiative rates. When a chromophore is placed near a gold nanoparticle, relaxation paths via either electron or energy transfer become available, thus increasing the rate of the non-radiative decay.

Gold nanoparticles can affect also the radiative rate of a chromophore.[131-132] Modification of the chromophore radiative rate by the gold nanoparticles can lead in optimal conditions to an enhancement of fluorescence intensity.[133] Change of the chromophore radiative rate is explained in terms of coupling of molecular and nanoparticle dipoles:[131] constructive interference of the dipoles corresponds to increased radiative rate and possible enhancement of fluorescence intensity. Both radiative and non-radiative decay rates are dependent on the distance between the particle and the chromophore and on the orientation of the chromophore dipole relative to the particle surface.[134]

There has been efforts in developing a general theory to explain both quenching and enhancement of fluorescence in gold-chromophore and gold nanoparticle-chromophore systems. One of these theories is based on radiating plasmons, a phenomenon called surface-plasmon-coupled emission.[135] It is proposed that energy from a chromophore is always transferred to a plasmon. Then, depending on the physical constraints of the sample, this plasmon either radiates or decays non-radiatively. Non-radiative plasmon decay corresponds to fluorescence quenching, which is observed with gold films and gold nanoparticles having absorption as the dominant feature of extinction. Radiative plasmons, and enhanced fluorescence can be observed when gold particles have scattering as the main feature of extinction. For gold nanoparticles, this presumes a core diameter larger than 40 nm.[135]

2.3.3 Porphyrinoid- and fullerene-gold nanoparticle assemblies

Combination of porphyrins and gold nanoparticles has yielded applications in photocurrent generation[136], catalysis[137] and anion sensing[138]. In porphyrin-functionalized gold nanoparticles, the fluorescence of porphyrins at short distances from the particle surface is quenched due to fast energy transfer.[124] A longer linker between the porphyrin and the particle diminishes energy transfer.[139] Porphyrin-functionalized gold nanoparticles with relatively long linkers can be used as building blocks for molecular organization for photocurrent generation: fullerene molecules become trapped between the porphyrin rings due to π-π interactions.[140-141] The organized assembly of porphyrins on gold nanoparticle surfaces is useful also in anion sensor applications, where sensitivity of porphyrins to certain anions is increased due to the controlled assembly.[138] Very strong interaction due to orbital overlap between porphyrin and gold nanoparticles is observed in porphyrins attached with multiple linkers parallel to the particle surface.[142]

There are fewer reports on phthalocyanine-functionalized gold nanoparticles than those for porphyrin-functionalized gold nanoparticles. Phthalocyanines can be used as sensitizers in photodynamic therapy for cancer treatment, where cytotoxic singlet oxygen destroys the cancer cells. Phthalocyanines absorb light at the red end of the visible spectrum, where human tissue has a high transmission. Photoexcited phthalocyanines transfer energy to oxygen, resulting in the production of singlet oxygen. Since phthalocyanine is hydrophobic, a delivery vehicle for its introduction inside the cells is required. The assembly of Zn-phthalocyanines on 4 nm gold nanoparticles with 12-atoms linker results only in weak energy transfer and the more impressive result from the assembly is an increased yield of singlet oxygen after photoexcitation of the phthalocyanine. Moreover, three-component assembly of phthalocyanine, gold nanoparticles and phase transfer agent is soluble in polar solvents, enabling delivery into cells.[143-144]

Porphyrins and phthalocyanines have been incorporated in films together with 14-18 nm gold nanoparticles for photovoltaic devices. The films were prepared using a self-assembly method. The gold nanoparticles increase the photocurrent of these systems and the proposed explanation is enhancement of the dye excitation due to localized surface plasmon resonance of the gold nanoparticles.[145-146]

Fullerenes show high affinity for gold nanoparticles and mixing fullerene with TOABr-protected gold nanoparticles produces large aggregates, where the individual particles are linked together by fullerenes.[147] Fullerenes modified with a thiol linker and attached to gold nanoparticles as mixed layers with dodecanethiols show energy transfer from photoexcited fullerene to the particle.[125] Assembly of these fullerene-functionalized particles in photoelectrochemical cells shows photocurrent generation, because the interaction of the electrolyte with the excited fullerenes leads to charge separation. The role of the gold nanoparticles is to promote charge separation and facilitate electron transfer within the film.[125] Somehow contradictory results have been obtained for fullerenes attached to 2 nm core diameter gold nanoparticles via a short phenyl linker, for which fluorescence enhancement was observed.[148] In studies for non-linear absorption of fullerene-functionalized gold nanoparticles, excitation at the surface plasmon band wavelength leads to energy transfer from the particles to fullerene.[149] Fullerenes clearly interact with gold nanoparticles, but the nature of the interaction seems to be dependent on the structure of the fullerene-functionalized particles.

3 Materials and methods

The experimental aspects of the work are described in this section, including the compounds and instruments used in the studies. Important experimental techniques for sample preparation were film deposition by Langmuir methods and ligand exchange reaction in the case of the porphyrinoid-functionalized gold nanoparticles. Spectroscopic methods were utilized for the characterization of both films and functionalized gold nanoparticles. The films were also characterized extensively from photoelectrical measurements. The microscope techniques used are also briefly described.

3.1 Compounds

Two different types of chromophores were required for the present work. The first set includes porphyrin, fullerene and porphyrin-fullerene dyad molecules that were known from previous studies to have good film forming properties. For the functionalization of gold nanoparticles, a method for modification of porphyrin molecules with a suitable linker was developed. Also a phthalocyanine with a linker for attachment to gold was used. Thiol-protected gold nanoparticles were utilized in the film preparation, whereas gold nanoparticles with a weakly bound ligand were used for the syntheses of chromophore-functionalized particles.

3.1.1 Molecules for film preparation

Porphyrin TBP (Figure 3.1A) has been synthesized by a condensation reaction of 3,5-di-*tert*-butyl benzaldehyde.[150] TBP contains *tert*-butyl-phenyl-groups, which improve solubility and reduce tendency for aggregation. Buckminsterfullerene is very hydrophobic, and cannot be used for film preparation by Langmuir film methods (described in detail in Chapter 3.2). Therefore a fullerene derivative with two carboxyl-groups, DAF, (Figure 3.1B) was used. The synthesis of DAF has been described in the literature.[151]

Porphyrin-fullerene dyads have been prepared by attaching a fullerene to a porphyrin with two linkers modified with malonate-groups that bind to fullerene.[150] Two different porphyrin fullerene dyads, denoted as DHD6ee and TBD6a (Figure 3.1C and D), were used. These molecules are similar in the number of linker atoms between the porphyrin and the fullerene

moieties. The fullerene and the porphyrin have face-to-face orientation due to the two linkers. The difference between the DHD6ee and TBD6a molecules is in the position of hydrophilic OH-groups. The dyad molecules are overall quite hydrophobic, but it has been shown that the OH-groups affect significantly their orientation at the air-water interface.[152] DHD6ee is oriented with the porphyrin moiety towards water, whereas TBD6a has the fullerene moiety located near the water surface.

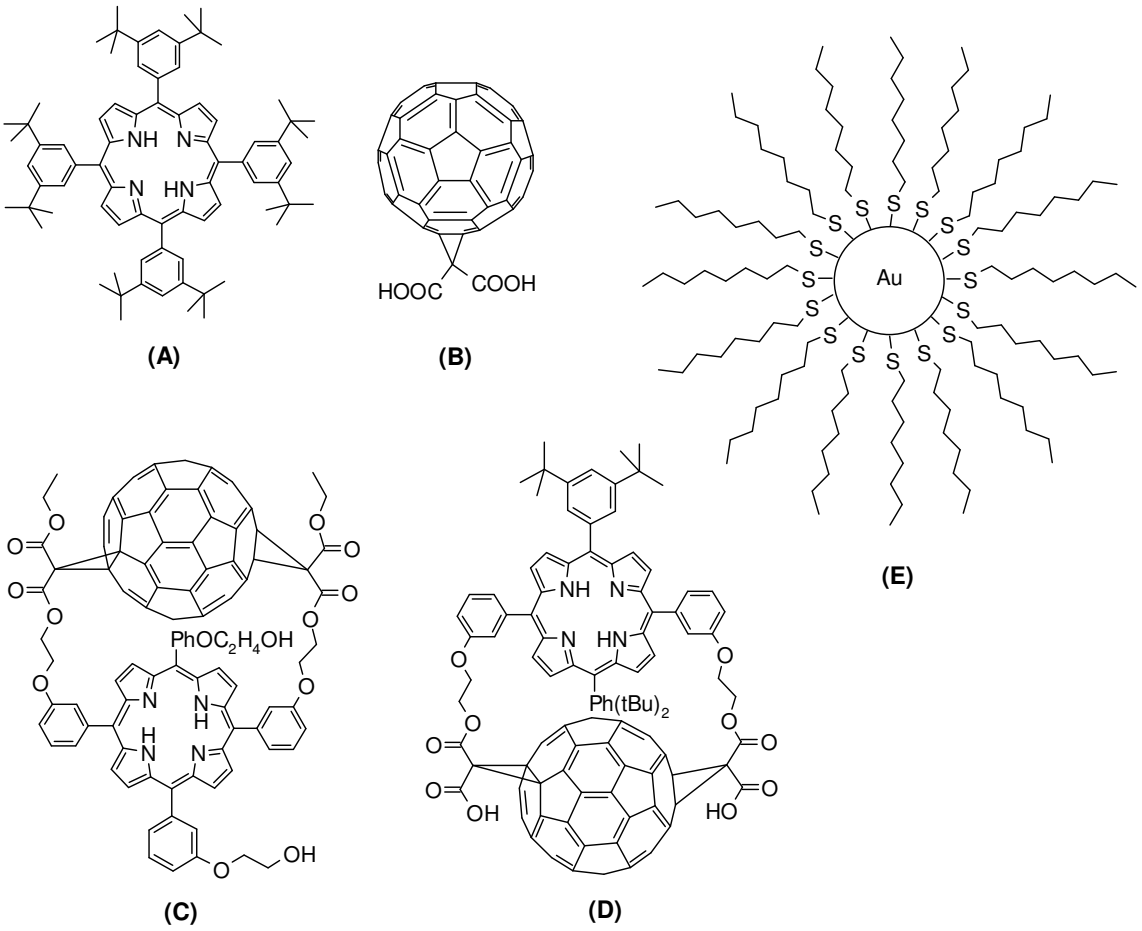

Figure 3.1. Molecular structures of (A) TBP, (B) DAF, (C) DHD6ee and (D) TBD6a and (E) schematic illustration of an octanethiol-protected gold nanoparticle (C_8SAu).

Octanethiol-protected gold nanoparticles were prepared with the two-phase Brust method[36], which can easily produce thiol-protected gold nanoparticles with core diameters from 1.5 to 20 nm[153]. The core size is determined by the thiol-to-gold ratio used in the reaction; the bigger the ratio is, the smaller the nanoparticle size. The Brust reaction begins by dissolving the gold precursor, $HAuCl_4$, in water. A toluene solution of a phase transfer agent, tetraoctylammonium bromide (TOABr) is added and the $AuCl_4^-$ ions are transferred to the toluene phase. After this, thiol is added, which forms a polymer with the gold precursor[41]. As a final step, an aqueous

solution of reducing agent, $NaBH_4$, is added and the gold nanoparticles are formed in toluene. After washing and fractional precipitation, the particles are ready for use. The prepared octanethiol-protected gold nanoparticles C_8SAu have core diameters of 2 or 3 nm according to transmission electron microscope (TEM) images. A schematic illustration of an octanethiol-protected gold nanoparticle is shown in Figure 3.1E. In reality the surface of gold nanoparticles is not smooth, but consists of planes and edges formed by gold atoms.[154]

3.1.2 Covalent attachment of porphyrinoids to gold nanoparticles

Thiols readily bind to gold nanoparticles, making them popular as protecting layers. Other sulfur-compounds such as disulfides, thioethers or thioacetates can also stabilize gold nanoparticles.[15] Thioacetates form similar bonds to gold as thiols due to the cleavage of the acetyl-group in contact with gold surfaces, but their reactivity is lower compared to that of thiols.[155] On the other hand, thioacetates are easier than thiols to prepare and handle.

A general route for formation of a thioacetate terminated linker starting from a hydroxyl-group is shown in Figure 3.2. The linker formation includes two fairly simple reaction steps that have reasonable yields.[IV]

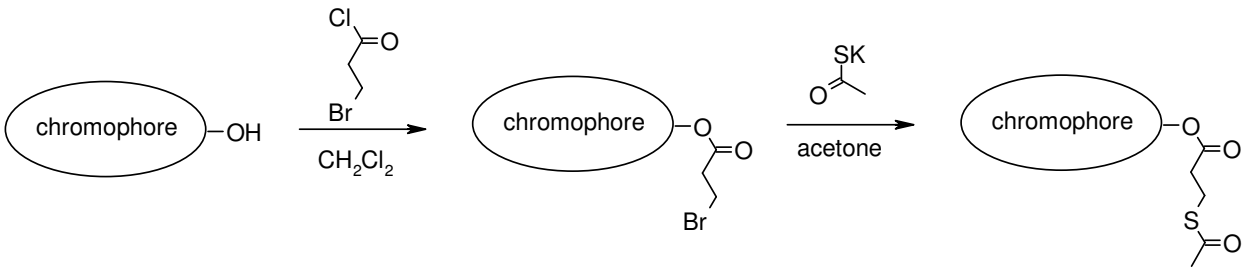

Figure 3.2. Reaction scheme for formation of thioacetate terminated linkers from hydroxyl-groups via two reaction steps.

The reaction scheme presented was used for the preparation of thioacetate porphyrins *cis*-Por and *trans*-Por (Figure 3.3A and B).[IV] These modified porphyrins have two similar linkers but on different positions of the porphyrin core. In addition to thioacetate porphyrins, thioacetate phthalocyanine Pc[156] (Figure 3.3C) was used for preparation of chromophore-functionalized gold nanoparticles.[V]

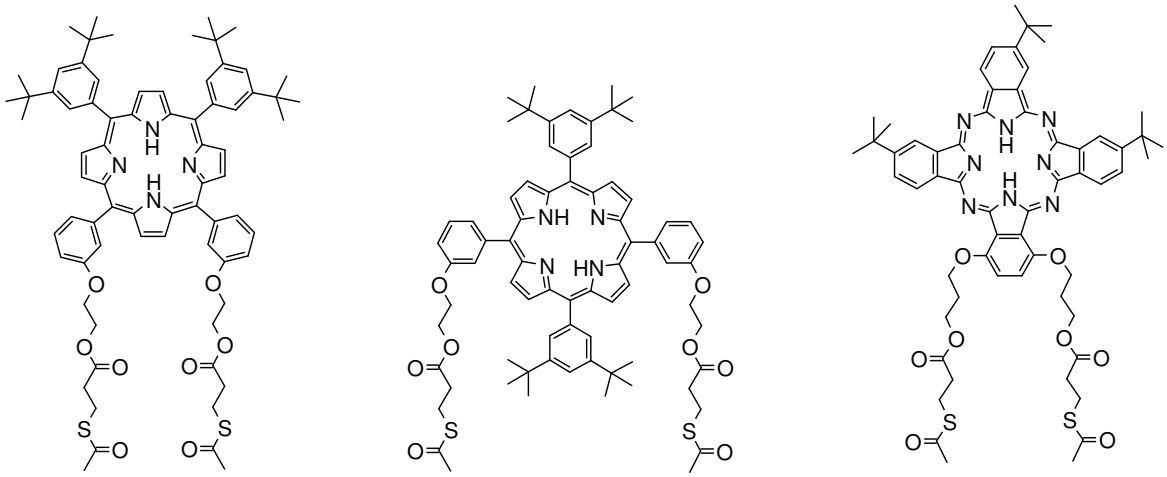

Figure 3.3. Molecular structures of compounds used for covalent attachment to gold nanoparticles (A) *cis*-Por, (B) *trans*-Por and (C) Pc**.**

Gold nanoparticles protected with TOABr molecules were prepared with a method similar to C_8SAu, except that no thiol was added and the amount of TOABr used in the reaction was higher. The TOABr-protected gold nanoparticles have a core diameter of approximately 5 nm, as determined by TEM. In contrast to C_8SAu, which can be dried and redissolved as any chemical compound, TOABr-AuNP were kept in toluene solution in order to prevent them from forming aggregates.

The porphyrinoid-functionalized gold nanoparticles were prepared via a ligand exchange reaction, where the loosely bound TOABr ligands are partially exchanged by porphyrinoids that bind covalently to the particle surface. Thioacetate porphyrinoids were stirred for 24 h with TOABr-AuNP in a toluene solution. An excess of the thioacetate porphyrinoids was used to obtain as high a surface coverage as possible. The unreacted thioacetate porphyrinoids were separated from the reaction mixture using size-exclusion chromatography. A schematic illustration of the structure of a phthalocyanine-functionalized gold nanoparticle[V] is shown in Figure 3.4.

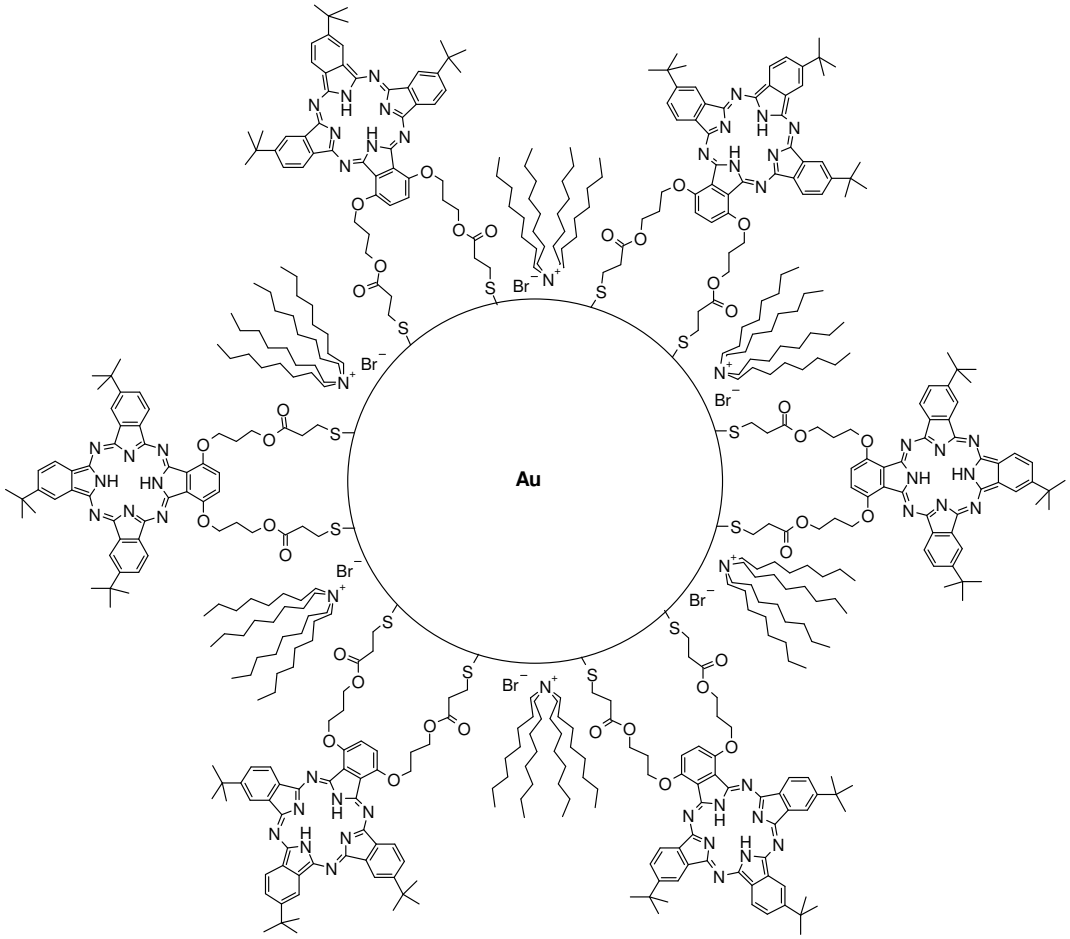

Figure 3.4. Schematic illustration of a phthalocyanine-functionalized gold nanoparticle. Gold nanoparticle core size is not in proportion to the size of the phthalocyanine molecules, and ratio and packing density of TOABr and phthalocyanine molecules are not represented accurately.

3.2 Film preparation

Well-controllable molecular film preparations can be achieved with Langmuir methods. Langmuir films, also called floating monolayers, are prepared by spreading amphiphilic molecules on a water surface from an organic solvent. As the solvent evaporates, the molecules are left floating on the water subphase. Langmuir films are formed in a trough, which is limited from one or two sides by barriers sliding along the trough edges. With these barriers, the molecules on the water surface are compressed to a smaller area, leading to an increase in surface pressure and to a decrease in the mean molecular area (that is, area per molecule). Ideally, four phases can be distinguished during compression. The first is a gaseous phase, Figure 3.5A. As the organization of the molecules increases, a liquid phase, Figure 3.5B, is

observed. Full organization is reached when a solid phase is formed, Figure 3.5C. After further compression, the film collapses and organization is lost.[157-158]

Films that are deposited on a solid substrate by moving the substrate vertically from air to water (or *vice versa*) are called Langmuir-Blodgett (LB) films. An alternative method of transferring films from the water surface to a substrate is the Langmuir-Schäfer (LS) method, where the substrate is lowered parallel to the water surface until it is in contact with the film and then lifted up. [157-158]

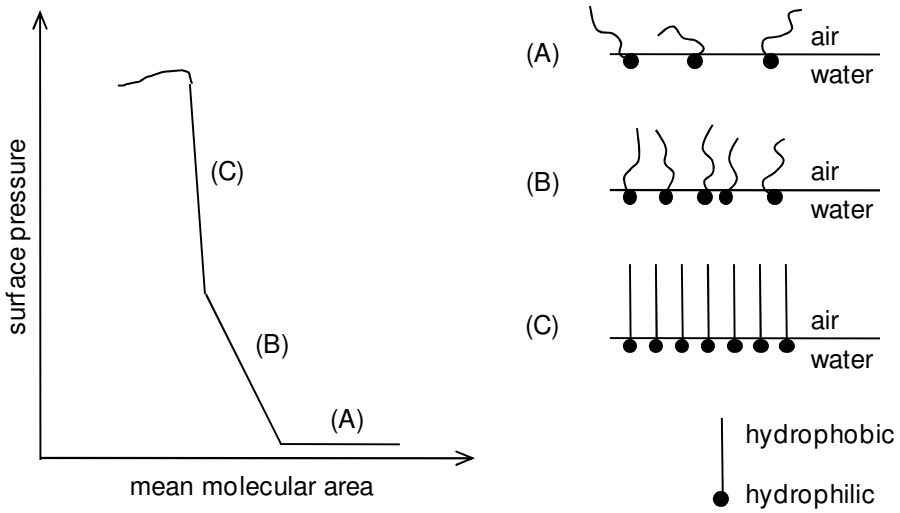

Figure 3.5. Schematic surface pressure-mean molecular area isotherm and organization of amphiphilic molecules at the air-water interface during compression proceeding from point (A) to (C).

Ideally, Langmuir films are formed employing amphiphilic molecules. Hydrophobic molecules will float on the water surface, and in some cases a Langmuir film is formed, though organization of the molecules is not well controlled. These Langmuir films are often rigid, and thus the LS method is preferable for film deposition on solid substrates. It is possible to prepare LB films of hydrophobic molecules by mixing them with an amphiphile in an appropriate molar ratio, but this might lead to the formation of island-like films due to poor mixing of the two compounds.

A Langmuir film of pure TBP is so rigid that film deposition is not at all possible. When TBP is mixed with an amphiphile, octadecylamine (ODA), it can be deposited as a LB film at a molar ratio of 10% of TBP in ODA. LS deposition can be done with 30% TBP films. DAF films were deposited as pure LS films. The optimal LB deposition of the porphyrin-fullerene dyad films is carried out with low molar ratios, ~10%.[152] On the other hand, LS deposition can be applied on pure dyad films. DHD6ee films were deposited as 10% LB films and TBD6a as 100% LS films.

The C_8SAu films were prepared either as 2% LB films or as pure LS films. Glass plates were used as substrates for the optical measurements, and indium tin oxide (ITO) covered glass plates for the photoelectrical measurements.

Films of PHT and C_6SAu were prepared on ITO plates for the photoelectrical measurements. The PHT layer was deposited by the LB method with a 60% molar ratio of PHT in ODA. The surface pressure for the PHT deposition was 20 mN m^{-1} and the subphase was a phosphate buffer containing 0.5 mM Na_2HPO_4 and 0.1 mM NaH_2PO_4 in MilliQ water. The core diameter of the C_6SAu particles was estimated to be approximately 3 nm from absorption spectrum measured in toluene. The C_6SAu LB deposition was possible, when a mass ratio of 80% of C_6SAu in ODA was used. The C_6SAu layer was deposited at a surface pressure of 7 mN m^{-1} and phosphate buffer was used as a subphase.

3.3 Spectroscopic measurements

Spectroscopic methods refer here to measurements related to interaction of matter with light. The wider definition of spectroscopy is measurement of a property as a function of wavelength or frequency. Time-resolved measurements were used in order to find out the characteristic timescales of the photoinduced processes. Different measurement setups are required for different timescales. Time-resolved absorption on the ps-timescale was measured with a pump-probe setup, whereas a flash-photolysis setup was used when resolution on the µs-timescale was needed. Two time-resolved fluorescence methods were also used: up-conversion on the ps-timescale and time-correlated single photon counting (TCSPC) on the ns-timescale. Here only the pump-probe and TCSPC methods are described in more detail, because these methods were mainly used. In addition, the principal difference of the time-resolved fluorescence (or absorbance) methods is not in the measured quantity, but in the technical implementation of the measurement.

3.3.1 Absorption and fluorescence spectra

Film deposition was monitored with absorption measurements. Absorption spectra of the functionalized gold nanoparticles were measured to determine how well the functionalization had proceeded. Absorption spectra were also used for selecting the excitation wavelength for example in steady-state fluorescence measurements and in photoelectrical measurements.

Steady-state fluorescence spectra were used for studying the interaction between two layers. Porphyrin is fluorescent and changes in the relaxation of excited porphyrin caused by gold nanoparticles will be seen as a modification of fluorescence intensity. Porphyrin-fullerene dyads also show fluorescence, which is effected by a gold nanoparticle film. For solutions of porphyrinoid-functionalized gold nanoparticles, emission quenching was used as an indication of the attachment of the chromophores to the particles.

3.3.2 Time-resolved fluorescence

Fluorescence lifetimes on ns-timescale were measured using the TCSPC system. Time-resolved fluorescence measurements on ps-timescale were carried out using the up-conversion setup described elsewhere[159]. The scheme of the TCSPC measurement is shown in Figure 3.6. The sample is excited by a laser pulse, and the same laser pulse is used as a trigger pulse for the time-to-amplitude converter (TAC). The triggering pulse starts the generation of a linearly rising voltage in the TAC and the pulse from emitted photon stops the rising potential in the TAC. The emitted photons are detected with a photomultiplier tube, which works in photon counting mode and thus produces an electrical pulse after each detected photon. Because the rise of TAC output voltage is linear in time, a certain output voltage corresponds to a certain delay time, Δt, between the excitation pulse and the emitted photon. The output voltage of TAC ($U(\Delta t)$) as a function of the delay time is processed by the multichannel analyzer (MCA), where each channel is associated to some voltage interval and therefore to some delay time interval. Each output voltage value adds one to the value stored at the corresponding channel. For example, the time step of the instrument can be set to 16 ps and then each channel stores the counts at this resolution. The measurement results, after repeated excitation pulses, in a decay curve with number of counts as a function of delay time. The time resolution of the instrument can be found out by measuring the instrument response function (that is, the decay profile of scattering of the excitation pulse), and for the used setup it was ~100 ps.

The fluorescence decays obtained from the TCSPC measurements were fitted with mono- or multi-exponential functions to obtain fluorescence lifetimes. Porphyrin fluorescence lifetime can be monitored with this measurement, and interaction of porphyrins with gold nanoparticles results in a change of fluorescence lifetime.[I,II] The effect of attachment of porphyrinoids to gold nanoparticles on their fluorescence lifetimes was studied with the TCSPC method.[IV,V] Another measurement type, in addition to measuring single decay curves at a chosen wavelength, is the determination of decay associated spectra (DAS). This measurement is useful for samples where

there are more than one emitting species present. Fluorescence decays at a chosen wavelength range are measured so that the collecting time is the same for each wavelength. As a result, the number of emitted photons at each wavelength can be compared, as well as the lifetimes. When the obtained decays are fitted simultaneously, each of the emitting species will show characteristic fluorescence lifetime and spectral shape. Porphyrin-fullerene dyads have many emitting species, and the effect of gold nanoparticles on the dyad fluorescence was studied by measuring the decay associated spectra.[III]

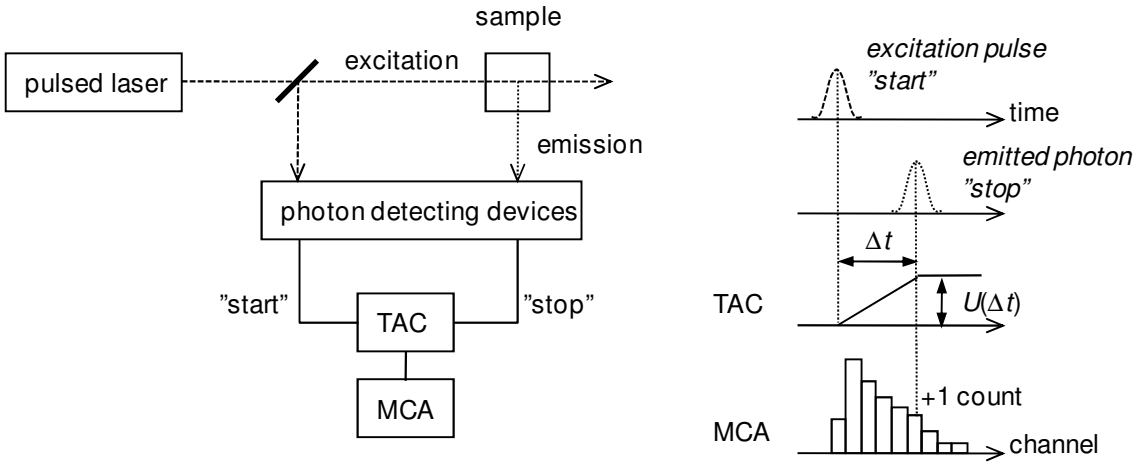

Figure 3.6. Scheme of the time correlated single photon counting (TCSPC) setup. TAC is the time-to-amplitude converter and MCA is the multichannel analyzer. Figure modified from Ref. 159.

3.3.3 Time-resolved absorption

The general idea of time-resolved absorption measurements is to monitor the change in the absorption spectrum of the sample at different times after excitation. Time-resolved absorption measurements on ps-timescale can be done with the pump-probe measurement setup, as shown schematically in Figure 3.7. A description of the time-resolved absorption measurements on µs-timescale employing a flash photolysis setup can be found elsewhere[159]. In the pump-probe setup, the base pulses come from a fs-pulsed laser. The base pulses are split between a white continuum generator and a second harmonic generator (SHG). In the setup used, the wavelength of the base pulses was 800 nm and the second harmonic used was 400 nm. The beam from the SHG is called the pump, that is, the excitation beam and it is guided into a delay line. The delay line is built with a moving mirror, whose position determines the path length of the pump beam and thus the relative delay time between the pump and the probe pulses. The pump beam is focused on the same spot in the sample as the signal beam. The beam from the white continuum

generator is called the probe beam, and is used for monitoring the absorption spectra of the sample. The probe beam is further split into two parts, reference and signal. They both pass into the sample, the reference beam through unexcited spot and the signal beam through the same spot as the pump beam, and after that reach the spectrograph and the photo-detector. The spectrograph spreads the white light of the reference and signal beams into colourful spectra. The photo-detector records both the reference and signal spectra, and from those the absorption change due to the excitation is obtained. When several positions of the delay line are scanned and detected, raw data in the form of differential transient absorption spectra at different delay times is produced. The time dependence of the transient absorption signal at each wavelength is obtained from the raw data. The transient absorption decay curves are then fitted simultaneously with a multi-exponential model to get the decay component spectra.

The fast (< 1.2 ns) photoinduced processes of porphyrin and gold nanoparticle containing films could be monitored using the pump-probe technique.[II] Pump-probe method requires samples with high absorbance. In the case of LS films, this usually means tens of layers, which makes the sample preparation challenging. The photoinduced processes at the phthalocyanine-functionalized gold nanoparticles were also studied with pump-probe measurements.[V] Pump-probe is a useful tool for monitoring both decay of excited singlet states and formation of charge transfer states.

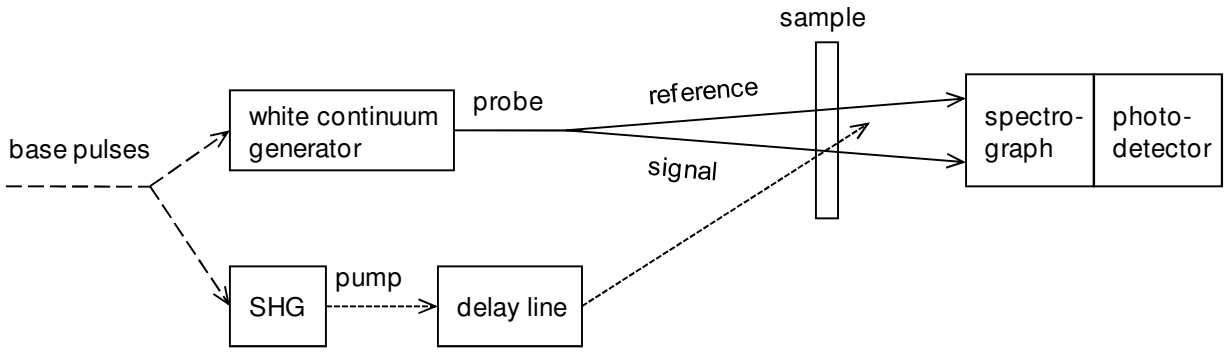

Figure 3.7. Simplified scheme of the pump-probe setup. SHG is a second harmonic generator. Figure modified from Ref. 159.

3.4 Photoelectrical measurement

Photoinduced charge transfer can be experimentally observed with two strategies: by measuring directly the number of moving charges (that is, the current) or by tracking the characteristic absorption of the charged species. The time-resolved Maxwell displacement charge

method (TRMDC)[160-162] has some advantages in detecting photoinduced charge transfer since it is very sensitive and can be applied to thin samples without destroying the photoactive films. The drawback of this method is the difficulty in calculating the absolute charge transfer efficiency.

The photovoltage measurement setup is shown schematically in Figure 3.8. The samples are prepared on glass substrates coated with conductive ITO. The photoactive films are insulated from the electrodes by ODA layers. The second electrode is an indium gallium (InGa) liquid metal drop, which is gently placed in contact with the sample. The sample is illuminated with light pulses. The photoexcitation leads to charge transfer between the donor and acceptor layers, inducing a voltage, U_{out}, between the electrodes, which is monitored as a function of time. There are no charges moving through the system because of the insulating ODA layers and the sample behaves as a capacitor (C ~ 200 pF). The time constant of the measurement circuit is determined by sample capacitance and amplifier input resistance R_{in}. The input resistance was typically 100 MΩ, which gives a time constant of ~20 ms. When the photovoltage is measured on a timescale much shorter than the circuit time constant, there is no significant discharging of the capacitor. Thus, the amplitude of the photovoltage is proportional to the number of charges and to the charge transfer distance. The sign of the photovoltage depends on the direction of electron movement: when electrons move in direction from the InGa electrode to the ITO electrode, the photovoltage is positive and *vice versa*. The decay of the signal is determined by the rate of charge recombination. There is a difference of ca. 0.5 V in the work functions of ITO and InGa. This built-in field in the samples can be reversed by applying an external voltage, U_{bias}, of -0.5 V. The change in external bias reveals if the photovoltage is independent of the external voltage, and thus actual charge separation, or dependent on the external bias and thus mainly caused by photoconductivity and field-induced charge shift.

The photovoltage measurements were applied to several bilayer films, including porphyrin-gold nanoparticle[I-II], fullerene-gold nanoparticle[I] and porphyrin-fullerene dyad-gold nanoparticle films[I,III]. As a result, conclusions on the directionality of the charge transfer[I-III], on the origin of the photovoltage[I-II], on the timescale of charge separation[I] and on the quantum efficiency of the charge transfer[II] could be made.

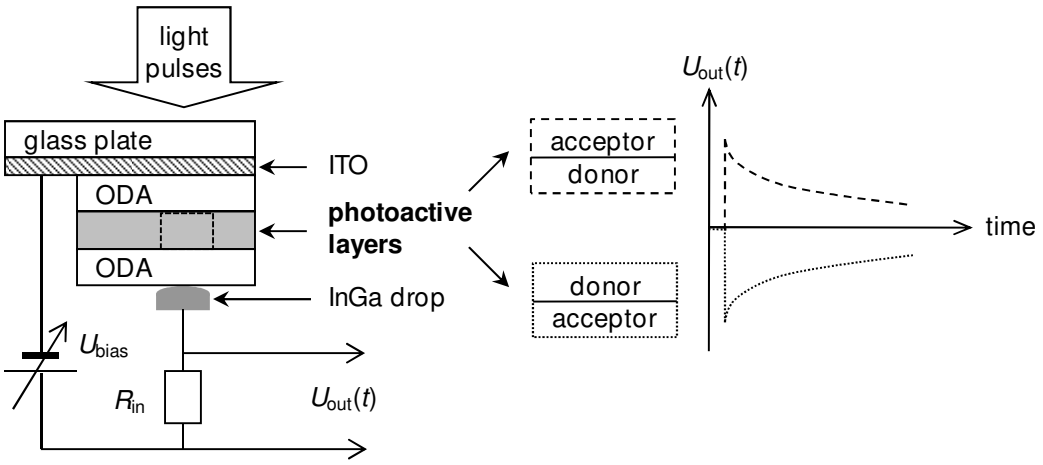

Figure 3.8. Schematic illustration of the TRMDC photovoltage measurement.

3.5 Microscope techniques

Transmission electron microscopy (TEM) was used for estimating the core diameter of gold nanoparticles.[I-IV] In a TEM measurement, an electron beam from an electron gun is guided into the sample using condenser lenses. The electrons are scattered from the sample atoms, mainly elastically, while passing through it. After this, the transmitted electrons are detected usually by a charge coupled device (CCD) camera. The spatial distribution of the scattered electrons is called electron diffraction pattern and provides information about the crystal structure of the sample, that is, arrangement of atoms. Besides diffraction pattern, TEM can yield a magnified image of the sample.[163]

Atomic force microscopy (AFM) was used for characterization of ODA-mixed DHD6ee and C_8SAu films on the nm-scale.[I] AFM is suitable for observing the roughness of both conducting and insulating samples. In a typical measurement setup, a tip is mounted on a cantilever. As the tip is placed in contact with the sample and moved across the sample surface, the cantilever is bent differently when the surface height changes. The displacement of the cantilever is due to repulsive forces between surface and tip. As a result, a map of force acting on the cantilever at different positions of the sample surface is obtained and this can be transformed into a topographic image. The cantilever displacement is usually monitored optically, using a light beam reflecting from the cantilever. AFM measurements can also be done in non-contact mode with an oscillating tip. The vibration frequency of the tip changes as the distance of the tip to the surface changes. This mode is based on attractive Van der Waals forces between the tip and the sample. Another AFM method is the tapping mode, where the resonating tip is brought into

contact with the sample surface and then retracted from the surface in cycles. Tapping mode is far less destructive method than contact mode.[164]

Fluorescence lifetime microscopy (FLM) maps fluorescence lifetime at different coordinates of the sample. In the used setup, the sample is moved and as a result 2D image of the fluorescence lifetime and intensity is obtained. TCSPC technique is used for data collecting. For a monolayer, possible holes and aggregates in the fluorescent film can be observed. In the case of bilayer films, the relative coverage of the films and the effect of the quenching layer on the fluorescent layer can be seen. FLM was applied to bilayers of TBD6a and C_8SAu to study the film structure on the μm-scale and the local variations of fluorescence lifetime.[III]

The above described microscope techniques (AFM, FLM) were used to characterize the selected thin films. The Langmuir films of TBD6a and C_8SAu on the water surface before deposition on solid substrate were studied with Brewster angle microscopy (BAM). BAM is based on reflection of polarized light at an interface of substances with different refractive indices. At Brewster angle, the reflection of the polarized light from the interface has a minimum. In a BAM measurement, there is no reflection from the air-water interface, but the monolayer changes the interface and the Brewster angle condition is not fulfilled anymore and light is reflected. The amount of the reflected light depends on the properties of the monolayer: thickness, roughness and anisotropy.[165-166]

4 Results and discussion

This chapter summarizes the most important results and findings of the studies presented in detail in publications I-V. First, the assembly of chromophores and gold nanoparticles in films and their photophysical interactions are discussed. Secondly, preparation of porphyrinoid-functionalized gold nanoparticles is introduced and their photoinduced processes are described.

4.1 Films

Assembly of film structures was performed using the Langmuir-Blodgett and -Schäfer techniques. Charge transfer in films was studied using the TRMDC photovoltage method. Spectroscopic methods were used to further characterize the film structures.

4.1.1 Assembly of film structures

The first step in assembling multilayer films of different compounds is to optimize the deposition of monolayers. It would be ideal to use pure films of the photoactive molecules but preparation of LB films from relatively hydrophobic molecules is difficult without the use of an amphiphilic matrix. On the other hand, the LS method can be applied to hydrophobic films, but the deposition is not always as controlled as in the case of LB films.

Thiol-protected gold nanoparticles have a hydrophobic character and their Langmuir film formation is enabled by the presence of the phase transfer agent employed in the synthesis.[167] The C_8SAu particles were prepared with the Brust method, which uses TOABr as the phase transfer agent. Another factor affecting the Langmuir film formation of the C_8SAu particles is their size dispersion. Particles obtained straight from the reaction were not suitable for film deposition but the size-fractioned particles readily organized in Langmuir films. Monodisperse particles arrange in ordered, close-packed crystalline structures.[168]

Absorption spectra of the three types of C_8SAu films used are shown in Figure 4.1A. The film of 3 nm C_8SAu particles shows a surface plasmon band at 520 nm. The film of 2 nm C_8SAu particles displays weaker surface plasmon band absorption due to the smaller particle size. The shape of the absorption spectrum of the 2 nm C_8SAu in ODA mixed film is similar to that of the 100% film, but the density of particles is smaller and therefore the absorption is also lower. AFM

images of the ODA mixed C_8SAu films show that the gold nanoparticles do not mix well with the ODA molecules but form separate domains with a relative surface coverage of 33%.[I]

TBP in ODA mixed film has an absorption maximum at 422 nm (Figure 4.1B). A DAF monolayer has typical absorption bands of fullerene at 210 and 260 nm and the tail of these bands is seen at longer wavelengths. Porphyrin-fullerene dyad films have an absorption maximum around 430 nm, as shown in Figure 4.1B for DHD6ee and in Figure 4.2A for TBD6a.

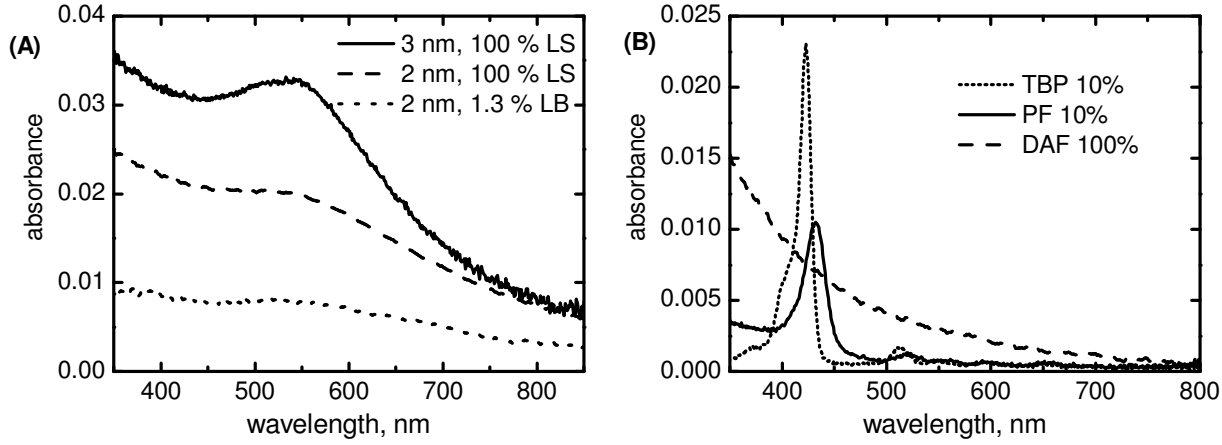

Figure 4.1. Absorption spectra of selected monolayers. (A) C_8SAu monolayers with different particle size and concentration and (B) monolayers of TBP, PF (DHD6ee) and DAF.

The quality of bilayer and multilayer deposition of photoactive materials was monitored by absorption measurements. Deposition was considered to be of good quality if the bilayer appeared to have both compounds in similar quantity as in their monolayers. An example of absorption spectrum measured after successful bilayer deposition is shown in Figure 4.2A for TBD6a and C_8SAu. For some measurements, the bilayers did not exhibit a high enough absorbance and multilayer deposition was necessary. The photoactive bilayers were separated from each other with three layers of ODA in multilayer films. The absorption increase during deposition of multilayers was linear for TBD6a and C_8SAu containing films, as shown in Figure 4.2B, indicating reproducible deposition of the layers.

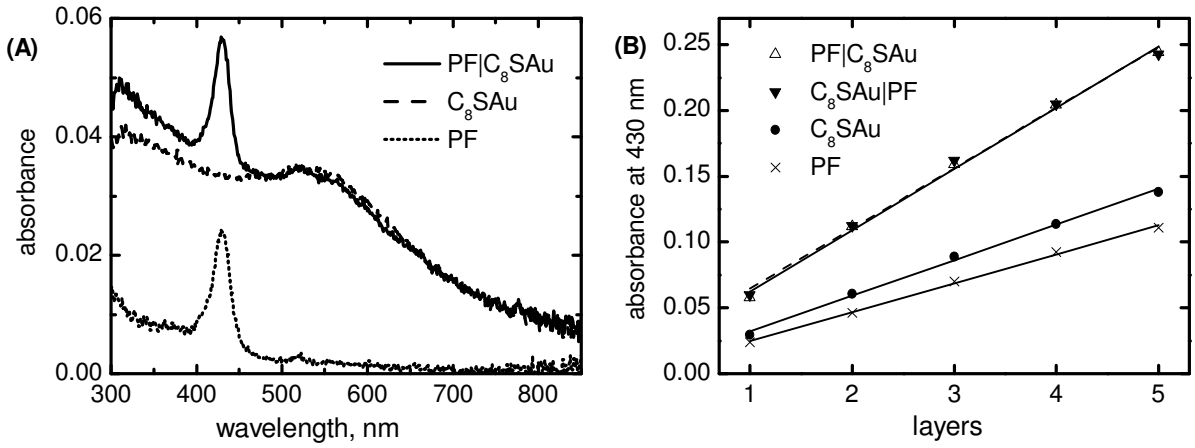

Figure 4.2. (A) Absorption spectra of PF|C_8SAu bilayer and the corresponding monolayers and (B) increase in absorption during multilayer depositions of PF and C_8SAu. The porphyrin-fullerene dyad used was TBD6a.

The amount of compounds transferred to a substrate can be monitored from absorption measurements, but microscope techniques are needed to reveal the film quality and structure on nm- and µm-scales. The structure of the C_8SAu|PF film, where both compounds are mixed in ODA, was studied on the nm-scale with AFM.[I] The bilayer has a complex structure because both films are dilute and C_8SAu and PF are present as separate islands in the ODA matrix. Nevertheless, the photoactive C_8SAu and PF covered areas partially overlap in the bilayer films. The PF|C_8SAu and C_8SAu|PF films, with both compounds as 100% layers, were characterized on the µm-scale with FLM.[III] The photoactive PF and C_8SAu layers have almost full coverage on each other.

4.1.2 Charge transfer in films

The TRMDC photovoltage method is a very sensitive measurement for observing charge transfer in thin films. Gold nanoparticle films do not generate significant photovoltage, but they can function as electron donors and acceptors to adjacent photoexcited chromophore films.

4.1.2.1 Porphyrin-gold nanoparticle bilayers

Porphyrin films show a weak negative photovoltage signal (Figure 4.3) due to a photoinduced charge shift caused by the electric field between the electrodes[161]. The photovoltage of ITO|ODAs|TBP|C_8SAu bilayer is positive (Figure 4.3), indicating electron transfer from the gold nanoparticles to the porphyrin layer[I-II]. At first, this observation seems to be in contradiction with the few reports on photoinduced charge transfer in chromophore-functionalized gold nanoparticles, where the latter usually acts as electron acceptor. From electrochemical studies, it

is known that gold nanoparticles can both donate and accept electrons.[75] The work function of gold nanoparticles in the metallic size regime, is approximately the same as for bulk gold, 5.3-5.5 eV against vacuum[169]. The HOMO level of porphyrin is 5.6 eV[170]. The energy levels of gold and porphyrin should allow hole transfer from porphyrin to gold nanoparticles, which is equivalent to electron transfer from the particles to the porphyrin. The reducing step in the synthesis of thiol-protected gold nanoparticles has been reported to leave the particles in a negatively charged state,[74] but exposure to air should remove this residual charge.[75]

Additional photovoltage measurements were carried out with poly(hexylthiophene) (PHT) films to clarify the electron donating and accepting properties of the gold nanoparticles. The HOMO level of PHT is 4.7-4.9 eV[170-171] and this compound is considered to be a good electron donor. The PHT layer absorbs light between wavelengths of 350 and 650 nm, with the maximum of the band located around 550 nm. Considering the energy levels of PHT in relation to the gold work function, hole transfer to gold nanoparticles should not be possible. Indeed, these bilayers show electron transfer from photoexcited PHT to the particles (Figure 4.3). It is thus clear that, depending on their companion, the gold nanoparticles can act both as electron acceptors and donors.

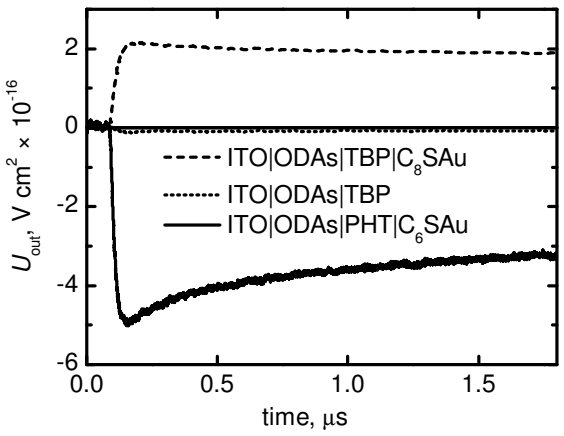

Figure 4.3. Photovoltage decays of TBP, TBP|C_8SAu and PHT|C_6SAu bilayers. The photovoltage amplitude has been divided with the photon density, because excitation wavelengths were 423 and 437 nm for porphyrin and PHT films, respectively. The molar concentrations of the molecules in ODA matrix are: TBP 10%, PHT 60%, C_8SAu 100%, and C_6SAu 80 mass-%.

Analysis of the dependence of the photovoltage amplitude on excitation energy density yields two parameters that describe the performance of the sample: saturation photovoltage U_0 and saturation energy density I_0. The fitting function is: [152]

$$U_{\text{out}} = U_0\left(1-\exp\left(-\frac{I_{\text{exc}}}{I_0}\right)\right), \tag{4.1}$$

where $I_0 = h\nu/\sigma$, I_{exc} is the excitation energy density, h is the Planck constant, ν is the frequency, and σ is the absorption cross section. The value of U_0 is the photovoltage at infinite excitation energy density. The saturation energy density can be used for calculating the absorption cross section of the species creating the photovoltage. In the case of bilayers of TBP and C_8SAu, the origin of photovoltage is the photoexcited porphyrin.[II]

The quantum efficiency of charge transfer in the TBP|C_8SAu bilayer is estimated from the saturation photovoltage:[162]

$$\varphi = \frac{n_{\text{TBP}^-}}{n_{\text{exc}}} = \frac{U_0 \times C \times D}{g \times S_{\text{el}} \times e \times d \times n_{\text{TBP}}}, \tag{4.2}$$

where $n_{\text{TBP-}}$ is the surface density of porphyrin anions formed, n_{exc} is the surface density of excited porphyrins, C is the capacitance of the sample, D is the total distance between the ITO and InGa electrodes, g is the amplifying factor of the instrument, S_{el} is the area of the electrode, e is the elementary charge, d is the distance of charge separation and n_{TBP} is the surface density of porphyrin molecules. The saturation photovoltage U_0 is used in the above equation, thus assuming that all the porphyrin molecules are excited. The quantum efficiency estimation is inaccurate due to the time resolution of the system. The initial charge transfer is usually very fast, but the time resolution of the TRMDC system is limited and the initial amplitude cannot be resolved. This means that the quantum efficiency is underestimated in the calculation. The lower limit of the quantum efficiency of the TBP|C_8SAu bilayer calculated from Equation 4.2, was 0.3%.[II]

The fluorescence of the TBP film is quenched by the adjacent C_8SAu layer, which can be partly explained by charge transfer between porphyrin and gold nanoparticles. Energy transfer is, however, the main reason for fluorescence quenching and will be discussed in detail in Chapter 4.1.3.

4.1.2.2 Fullerene-gold nanoparticle bilayers

The photovoltage of the ITO|ODAs|C_8SAu|DAF bilayer is negative (Figure 4.4) and thus electrons are transferred from gold nanoparticles to fullerene.[I] The HOMO level for fullerene is

6.0-6.2 eV against vacuum[172], which is higher than that for porphyrin and therefore hole transfer from photoexcited fullerene to gold nanoparticles can readily take place.

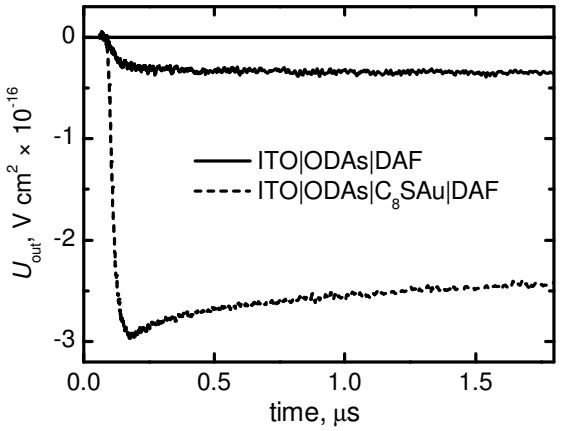

Figure 4.4. Photovoltage decays of DAF and C_8SAu|DAF bilayer. The photovoltage amplitude has been divided with the photon density at excitation wavelength of 434 nm. The molar concentration of C_8SAu is 2% in ODA and DAF film is 100%.

4.1.2.3 Porphyrin-fullerene dyads and gold nanoparticles

The photovoltage amplitudes of TBP|C_8SAu and C_8SAu|DAF bilayers indicate that gold nanoparticles are electron donors to photoexcited porphyrins and fullerenes. The porphyrin-fullerene dyads DHD6ee and TBD6a have hydrophilic groups either on the porphyrin or fullerene moiety, respectively. The dyads organize at the air-water interface due to the hydrophilic groups and form structures, where the porphyrins form a layer adjacent to the fullerene plane.[152] These organized porphyrin-fullerene dyad films generate photovoltage due to photoinduced electron transfer from the photoexcited porphyrins to the fullerenes. The photovoltage of the dyad layer is enhanced when the gold nanoparticle layer is placed near the porphyrin moieties of the dyad layer.[I,III] This is the case for the two different porphyrin-fullerene dyads, DHD6ee and TBD6a, as shown in Figure 4.5. The effect of gold nanoparticles placed near the fullerene moieties of the dyad layer is not as beneficial, because the photovoltage of these films is of opposite polarity compared to that of the dyad (Figure 4.5).

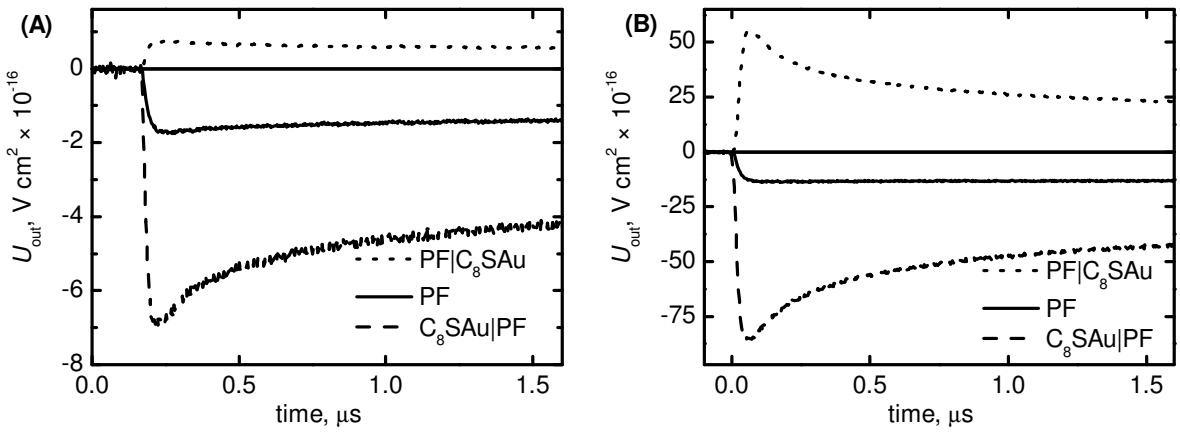

Figure 4.5. Photovoltage decays of PF dyad and gold nanoparticle bilayers (A) DHD6ee (10%) and C_8SAu (2 nm, 2%) and (B) TBD6a (100%) and C_8SAu (3 nm, 100%). The photovoltage amplitude has been divided with the photon density at excitation wavelengths of 432 and 430 nm for DHD6ee and TBD6a containing films, respectively.

There are two possible reasons for the increased photovoltage of the C_8SAu|PF films: either an increased number of charges or a longer charge separation distance. The number of separated charges is essentially dependent on absorption by the photoactive species. The dependence of the photovoltage amplitude on excitation energy density confirms that the dyad is the species creating the photovoltage of the C_8SAu|PF films.[I] This conclusion is also supported by results obtained using an excitation wavelength of 530 nm, where the absorption cross section obtained from the fit of photovoltage dependence on excitation energy density corresponds to that of the dyad.[I] At this wavelength, the possible effect from the gold nanoparticles should be visible because their absorbance is higher than that of the dyad. Increased absorption of the sample is not thus a reasonable explanation for the enhancement of photovoltage, especially because the size of the gold nanoparticles is so small that their scattering is negligible compared to their absorption. It can be concluded, therefore that the enhanced photovoltage is due to the increased charge separation distance.

The excitation of porphyrin in TBD6a films leads to fast (< 100 fs) exciplex formation.[173] The charge-separated state can be reached from the exciplex intermediate. The dyad exciplex has a characteristic emission band in non-polar solvents at 700-900 nm[94] but in films, the exciplex emission is not very reproducible. The fluorescence of the TBD6a layer is partially quenched by gold nanoparticles in both C_8SAu|PF and PF|C_8SAu films at all emission wavelengths.[III] The fluorescence spectrum of TBD6a film is the sum of emissions of three species: porphyrin, fullerene and exciplex.[152] All these species have their characteristic lifetimes and spectral characteristics that can be studied by measuring the decay associated fluorescence spectra. DAS

measurements were used to study the effect of gold nanoparticles on the TBD6a exciplex emission.[III]

Unexpectedly, the TBD6a film has strong porphyrin emission bands at 660 nm and 720 nm. The lifetime of this porphyrin fluorescence is distributed to different values due to different local environments and organization of the molecules in the film. Based on the measured lifetimes, the 0.14 ns component in Figure 4.6A corresponds to porphyrin emission, the 0.46 ns to fullerene emission and the 1.5 ns to exciplex emission. For C_8SAu|PF film, the lifetimes of the emitting species of the dyad are decreased but the spectral characteristics of the different components remain the same (Figure 4.6B). This is in agreement with the enhanced photovoltage of the C_8SAu|PF film if two parallel mechanisms are considered: 1) gold nanoparticles help the dyad to proceed from the exciplex state to the charge separated state and 2) a hole is transferred from the porphyrin to the gold nanoparticle after charge separation in the dyad. Quantum efficiency of charge separation is less than 25% in a TBD6a film,[173] and thus mechanism 1) is feasible and results in an increased number of separated charges. Mechanism 2) indicates an increased charge separation distance.

The photovoltage signals of the PF|C_8SAu films are opposite in sign to those of the dyads (Figure 4.5). As already mentioned, the exciplex formation in the dyad is very fast and it most likely cannot be disturbed by the adjacent gold nanoparticle layer. The interaction of the fullerene moiety and the gold nanoparticle film seems to be quite strong, since the exciplex component in PF|C_8SAu (Figure 4.6C) has different characteristic compared to that of the dyad. Together with the change in the polarity of the photovoltage signal, this indicates that the gold nanoparticle film donates electrons to the fullerene moieties thus reducing the efficiency of charge separated state formation in the PF|C_8SAu films.

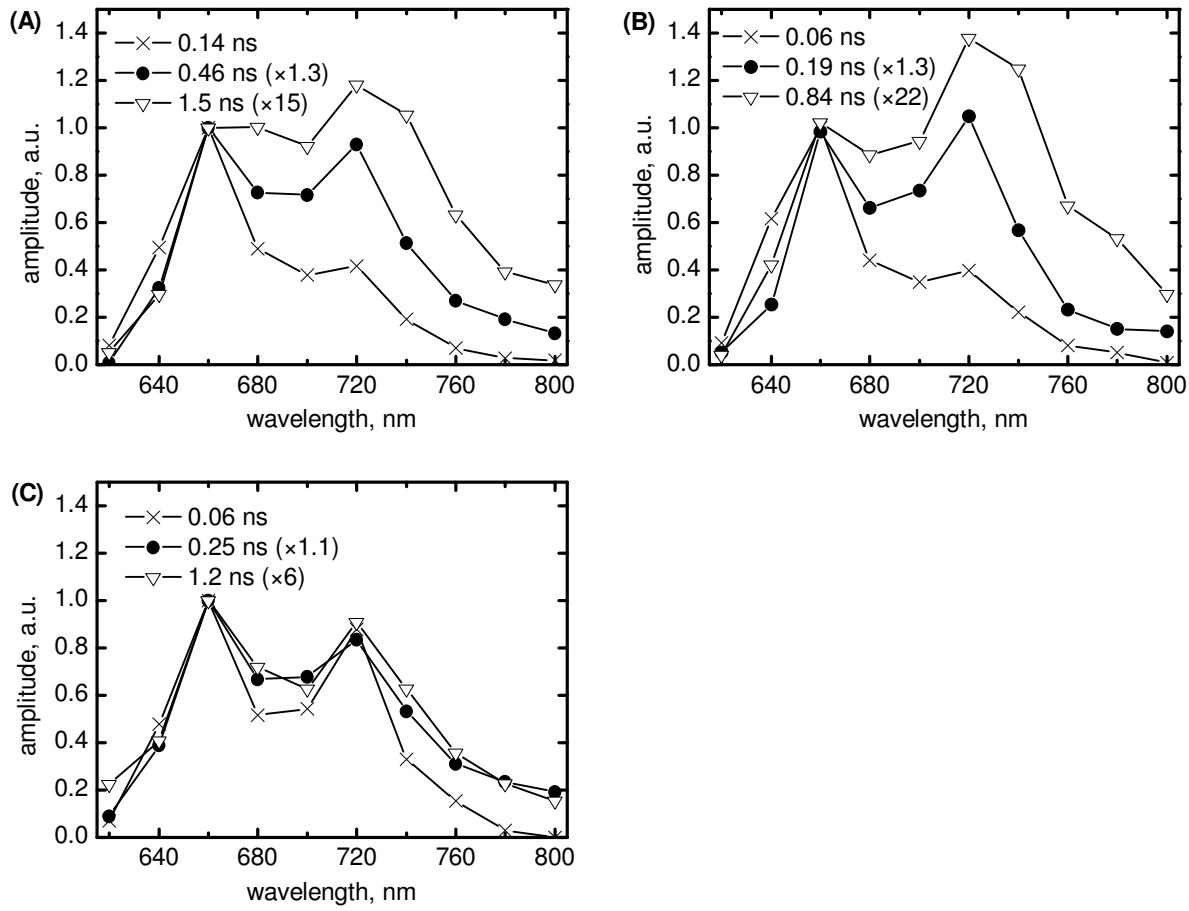

Figure 4.6. Normalized decay associated spectra of (A) PF, (B) C_8SAu|PF and (C) PF|C_8SAu multilayer films. Both TBD6a and C_8SAu films were 100%. Excitation wavelength was 405 nm.

It is well known that gold nanoparticles are capable of quenching excited singlet states of chromophores. The results with porphyrin-fullerene dyad films show that also intramolecular exciplex state can be quenched by gold nanoparticles. Moreover, the photovoltage amplitude and exciplex emission of the dyad are very sensitive to the positioning of the gold nanoparticle layer, either facing the fullerene or porphyrin moieties of the dyad film.

4.1.3 Energy transfer in porphyrin-gold nanoparticle films

4.1.3.1 Relative importance of energy and charge transfers

Photovoltage measurements demonstrate that charge transfer takes place in the porphyrin-gold nanoparticle bilayers but also resonant energy transfer can occur due to the overlap of porphyrin fluorescence and gold nanoparticle absorption spectra. Porphyrin fluorescence in the TBP|C_8SAu bilayer is strongly quenched, to 2% of the TBP monolayer fluorescence intensity.[II] The average fluorescence lifetime of the porphyrin is also reduced significantly, from 4.3 ns for a

TBP film to 0.3 ns for the TBP|C_8SAu bilayer.[II] The fluorescence decays measured with the TCSPC instrument are shown in Figure 4.7. Both energy and electron transfers are possible reasons for the observed quenching.

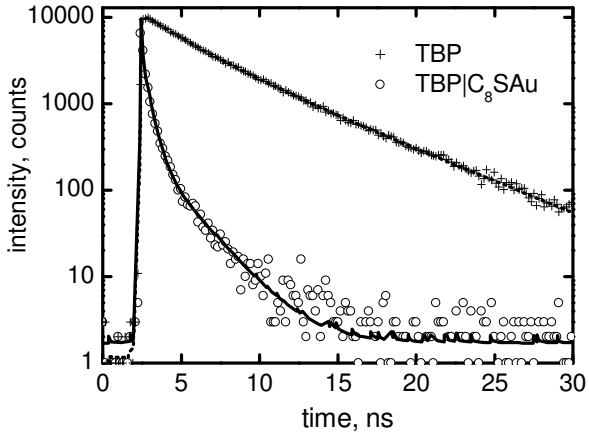

Figure 4.7. Fluorescence decay curves for TBP and TBP|C_8SAu films. The molar concentration of TBP is 30% in ODA and C_8SAu film is 100%. Excitation wavelength was 405 nm and monitoring wavelength 660 nm.

Time-resolved absorption measurements are useful in tracking species formed by photoinduced electron transfer, because radical ions have characteristic absorption bands. The pump-probe measurements require high absorbance of the samples and therefore multilayer films of TBP, C_8SAu and TBP|C_8SAu were prepared.[II]

The decay component spectrum of the C_8SAu film shows bleaching of the plasmon band at ~540 nm, with photoinduced absorbance on both sides of the bleach (Figure 4.8). A lifetime of ~2 ps is observed for the C_8SAu film, which can be attributed to an electron-phonon scattering process.[II] The decay component spectrum of the TBP film has two components, both corresponding to the first excited singlet state. The component with the longer lifetime, 690 ps, is too long to be fully resolved by pump-probe measurement. This is in agreement with the fluorescence lifetime of the TBP film. The 23 ps component probably originates from energy transfer between porphyrins in the TBP film. The decay component spectrum of the TBP|C_8SAu film has two components at ~2 and 20 ps. The shorter component clearly corresponds to the response from the gold nanoparticles and the longer to the porphyrin first excited singlet state. The lifetime of the porphyrin first excited singlet state is thus significantly shorter in the TBP|C_8SAu film compared with that of the TBP film. The photovoltage measurements indicate that the charge separated species in the TBP|C_8SAu film have lifetimes of microseconds, but such long living components were not observed in the pump-probe measurements.

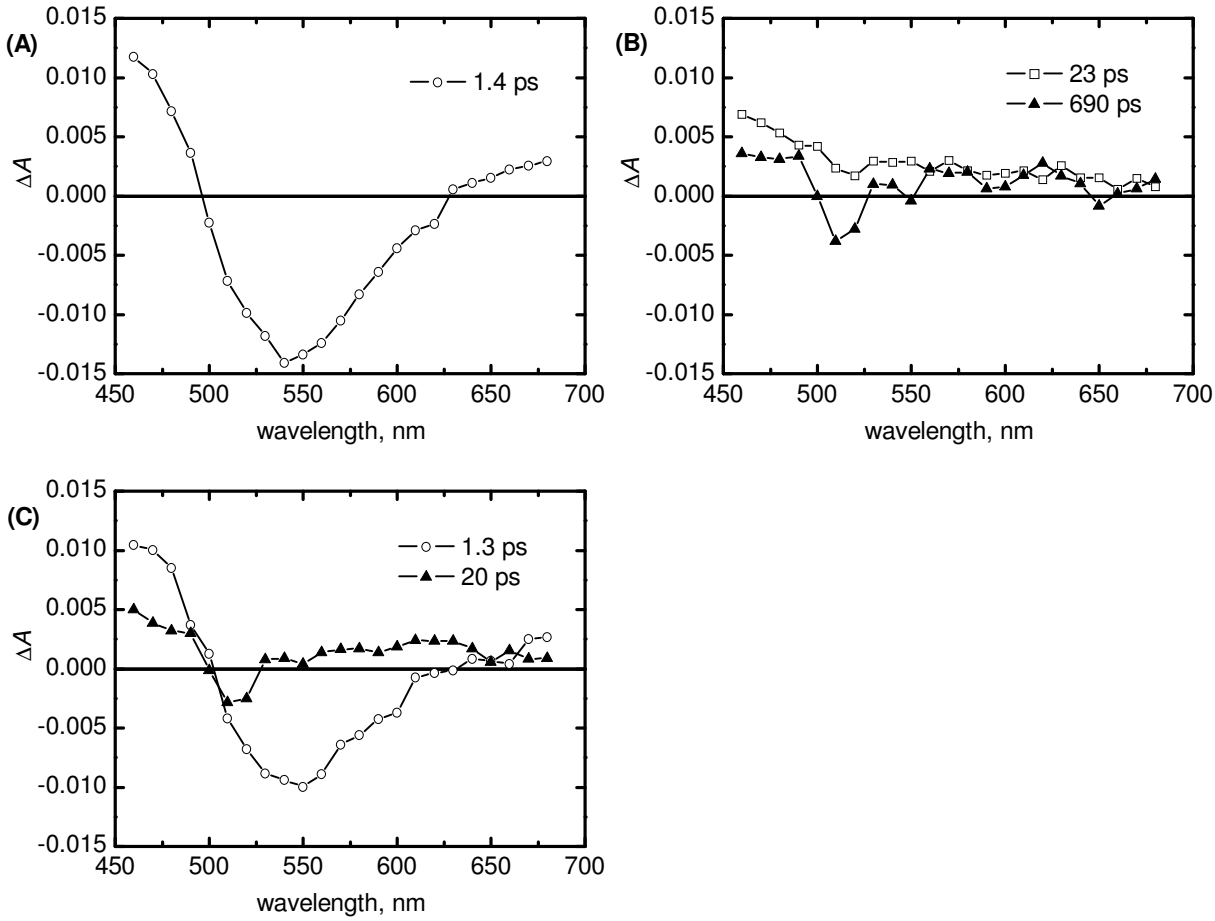

Figure 4.8. Decay component spectra obtained from global fitting of pump-probe decay curves for (A) C_8SAu, (B) TBP and (C) TBP|C_8SAu multilayer films. The molar concentration of TBP is 30% in ODA and C_8SAu film is 100%. Excitation wavelength was 420 nm.

The transient absorption of the TBP|C_8SAu film was too weak to be measured with the pump-probe technique in the NIR region, so this wavelength range was studied using flash photolysis measurements. In addition to the long-lived radical species, the long-lived triplet state of the porphyrin can be expected to be observed by this method. The porphyrin triplet state has an absorption band around 450 nm in the TBP film and this is significantly reduced in the TBP|C_8SAu film.[II] No proof for the presence of porphyrin radical ions was observed in these flash photolysis measurements. On the other hand, photovoltage measurements clearly show electron transfer from the gold nanoparticles to the porphyrins. The estimated lower limit of the charge transfer quantum efficiency obtained by this method is 0.3% (see Chapter 4.1.2.1). Taking into account the noise level of the flash photolysis setup and the absorption coefficient of the porphyrin radical anion, its absorption will not be distinguishable from instrumental noise if charge transfer efficiency is less than 10%. In conclusion, 10% of the excited porphyrins relax

via the triplet state in the TBP|C_8SAu films, less than 10% by hole transfer to the gold nanoparticles and more than 80% by energy transfer to the gold nanoparticles.

4.1.3.2 Distance dependence

Energy transfer to gold nanoparticles was found to be the major relaxation path for photoexcitation of porphyrins in the TBP|C_8SAu films and therefore, further analysis of this process was conducted. The efficiency of resonance energy transfer is dependent on the distance between the donor and acceptor according to:[127-128]

$$\frac{F_{\text{with acceptor}}}{F_{\text{without acceptor}}} = \frac{1}{1+\left(\frac{d_0}{d}\right)^n}, \tag{4.3}$$

where F is fluorescence intensity, d_0 is the critical distance, d is the distance between donor and acceptor and n is the parameter determined by molecular organization. At the critical distance, the relaxation by energy transfer is as efficient as through other relaxation routes. In the Förster mechanism $n = 6$ when energy is transferred between two isolated dipoles. For energy transfer from a point dipole to a layer, $n = 4$ and for layer-to-layer energy transfer $n = 2$.

Porphyrins are packed closely in the TBP films and energy transfer in the TBP|C_8SAu film is considered to take place between two layers. The distance between TBP and C_8SAu layers was changed by depositing ODA layers between them. The thickness of one ODA layer is estimated to be ~2.5 nm from the number of bonds. The distance between adjacent TBP and C_8SAu layers is taken as the length of the protecting thiol chain, ~1 nm. The fitting of data points from fluorescence quenching at different distances is shown in Figure 4.9, from which a critical distance of ~6.4 nm was obtained.[II]

As shown by the photovoltage measurements, charge transfer can occur in the TBP|C_8SAu bilayers. The photovoltage decay for films where the TBP layer was separated from the C_8SAu layer by one or three ODA layers was also measured. Three layers of ODA between the porphyrin and gold nanoparticle layers prevent charge transfer and one layer of ODA reduces the photovoltage amplitude to about half compared to a TBP|C_8SAu bilayer. Thus, there is some charge transfer trough one ODA layer, corresponding to a distance of 3.5 nm in Figure 4.9. The distance is probably too long for charge transfer to take place through the ODA layer, but most likely the deposition of ODA is uneven and TBP and C_8SAu layers are in direct contact with each other.

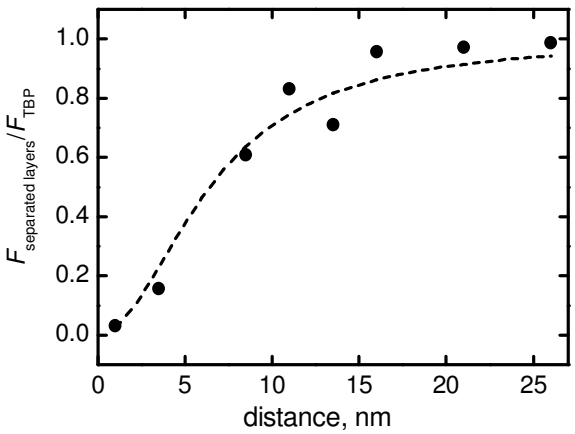

Figure 4.9. Fluorescence quenching as a function of distance between the TBP and C_8SAu monolayers.

4.2 Porphyrinoid-functionalized gold nanoparticles

The preparation of thiol-protected gold nanoparticles is relatively simple and there are many alternative synthetic approaches available. The synthesis gets more complicated if bulkier molecules are used as the protecting layer. Aliphatic thiols can pack tightly on the surface of the gold nanoparticle and as a consequence, aggregation is well prevented. The packing is not as tight with bulkier molecules, which can yield to insoluble materials due to aggregation of the gold cores.

Thioacetates are easier to handle and prepare than thiols and they form similar bonds to gold as thiols since the acetyl-group cleaves on gold surfaces.[155] The downside of the easier handling is lower reactivity of thioacetates towards gold and a higher concentration compared to thiols is needed for reaction.[155] Formation of porphyrin-functionalized gold nanoparticles proved to be quite challenging because the synthetic chemistry, in contrast with the behaviour with thiols, failed with the big thioacetate porphyrins. Thiol exchange would have been one choice but the exchange of a small thiol by a bulkier one would have required very high excess of the incoming thiol and the exchange number would be probably very low. On the other hand, gold particles protected with a weakly bound ligand allow an easy exchange of the ligand by the porphyrin thioacetates. Therefore, TOABr-protected gold nanoparticles were chosen for the ligand exchange reactions.

There are some advantages of using the ligand exchange route for the attachment of chromophores to gold nanoparticles compared to the traditional Brust reaction[36], for instance, the chromophore to be attached is not exposed to acidic or reducing conditions. The attachment

process using TOABr-AuNP should therefore be suitable for many types of molecules. A drawback of the method is the presence of TOABr impurity in the final chromophore-functionalized gold nanoparticles.

Porphyrinoid-functionalized gold nanoparticles[IV-V] were thus obtained by a ligand exchange reaction, where porphyrinoid thioacetates attach to TOABr-protected gold nanoparticles. Excess of porphyrinoid thioacetates was used and the unattached molecules had to be removed after the reaction. This was done using size-exclusion chromatography since the free porphyrinoids are smaller than the functionalized gold nanoparticles. The progression of the exchange reaction could be monitored by thin layer chromatography; TOABr-AuNP are immobilized on the silica plate, while the porphyrinoid-functionalized gold nanoparticles move as a tailing spot. The modification of the protecting layer of the nanoparticles thus affects their polarity, though no big changes in solubility were observed.

Absorption spectra of porphyrinoid-functionalized gold nanoparticles are shown in Figure 4.10A. The absorption spectrum of porphyrin-functionalized gold nanoparticles is composed of the porphyrin Soret-band at 420 nm and the surface plasmon band of gold nanoparticles at 526 nm (Figure 4.10A). The porphyrin Soret-band is not affected by attachment to the nanoparticle and its shape and position remain the same as for the *cis*-Por or *trans*-Por toluene solutions. The plasmon band seems to be slightly broader in porphyrin-functionalized gold nanoparticles compared to TOABr-AuNP. TEM images of *cis*-Por-AuNP show that the size of the gold core is not significantly affected by the ligand exchange reaction.[IV]

The phthalocyanine Soret-band of Pc-AuNP is observed at ~340 nm and has similar shape and position as that of Pc (Figure 4.10B). By contrast, broadening of the phthalocyanine Q-band is observed for Pc-AuNP compared to that of Pc. The Q-band broadening is due to aggregation[174] of the phthalocyanine molecules attached to the nanoparticles. Pc-AuNP have a surface plasmon band at 519 nm, and it has same shape and position as that of TOABr-AuNP before ligand exchange.

Several batches of TOABr-AuNP were prepared from the same reactants and with similar conditions, but their synthesis is extremely sensitive to small variations in reaction conditions. This is seen as a variation of the bandwidth and the position of the surface plasmon band between 520-534 nm.

Absorption spectra of the porphyrinoid-functionalized gold nanoparticles can be used in estimating how many molecules are on average attached to one gold core. This is a very rough estimation because the particle is approximated as a sphere with a diameter of 5 nm and the size distribution or surface structure are not taken into account. Based on molar absorption coefficients of thioacetate porphyrinoids and TOABr-AuNP, there are 30, 23 and 60 *cis*-Por, *trans*-Por and Pc molecules, respectively, attached to one gold core. The difference in the number of porphyrins per nanoparticle for *cis*-Por-AuNP and *trans*-Por-AuNP is most likely caused by different position of the linkers, which causes different packing of the molecules on the particle surface.

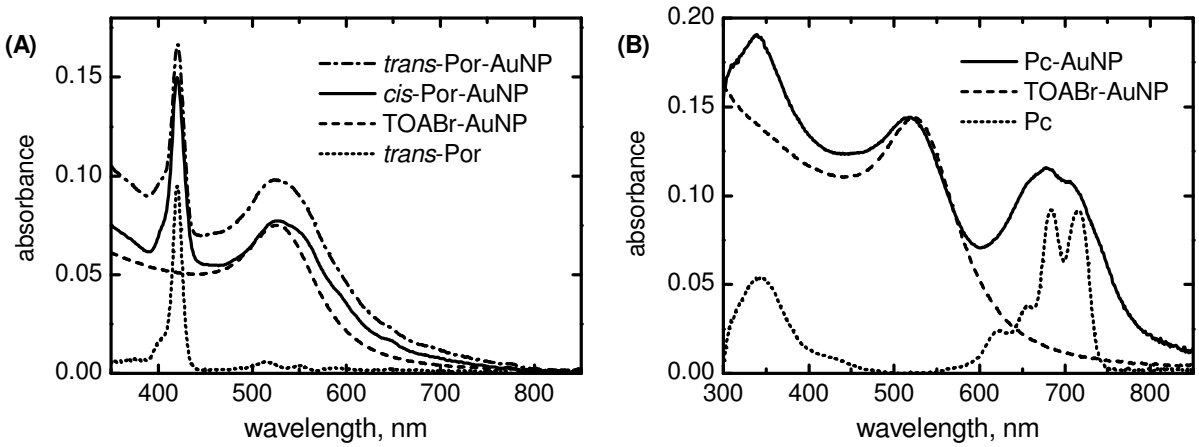

Figure 4.10. Absorption spectra of (A) porphyrin-functionalized gold nanoparticles and (B) phthalocyanine-functionalized gold nanoparticles.

4.2.1 Energy transfer in porphyrinoid-functionalized gold nanoparticles

Fluorescence of the porphyrinoids is quenched after attachment, as shown in Figure 4.11. In the case of porphyrin-functionalized gold nanoparticles, the quenching is to less than 20% compared to porphyrin solution with similar absorbance at the excitation wavelength (Figure 4.11A). In phthalocyanine-functionalized gold nanoparticles the quenching is close to ~10% (Figure 4.11B). This quenching raises two questions: what is the reason for fluorescence quenching and where the remaining observed fluorescence comes from? The quenching mechanism cannot be extracted from the fluorescence spectra, but the absorption spectrum of Pc-AuNP indicates aggregation of the phthalocyanines on the particle surface. The close packing of phthalocyanines can cause self-quenching of the fluorescence.

The two anticipated mechanisms of fluorescence quenching in these systems are energy and charge transfer to the gold cores. Fluorescence lifetime measurements can be used to investigate

the origin of the remaining fluorescence. Fluorescence of porphyrin-functionalized gold nanoparticles shows two-exponential decay with shorter lifetimes of 20 and 40 ps for *trans*-Por-AuNP and *cis*-Por-AuNP, respectively and a longer lifetime of 9.8 ns for both.[IV] The longer component has the same lifetime as that of *cis*-Por or *trans*-Por in solution. The fluorescence lifetime of Pc-AuNP is 4.6 ns, which is very similar to the lifetime of Pc in toluene, 5.0 ns.[V] The longer lifetime for porphyrin-functionalized gold nanoparticles is attributed mainly to free, unattached porphyrins resulting from incomplete purification process. This conclusion is based on the observation that an increased number of runs through the size exclusion column increased the apparent fluorescence quenching. The problem was that after certain number of column purification runs, the particles became unstable. By contrast, the phthalocyanine-functionalized gold nanoparticles were thoroughly purified from unattached Pc molecules. Thus, there has to be some other explanation than free phthalocyanines for the remaining fluorescence of Pc-AuNP. It is assumed that some of the attached phthalocyanine molecules on the gold nanoparticle surface are packed differently and therefore have intact fluorescence lifetime.

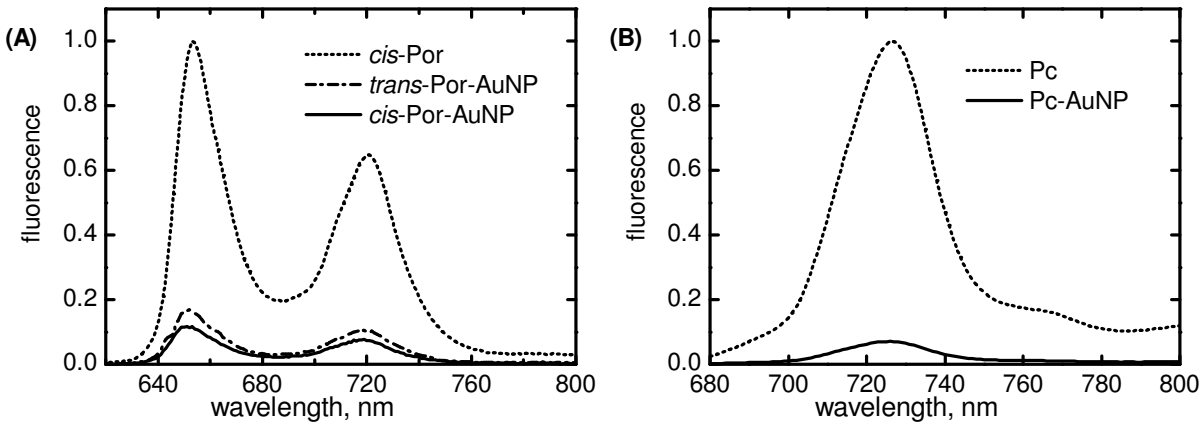

Figure 4.11. Fluorescence spectra of (A) porphyrin-functionalized gold nanoparticles and (B) phthalocyanine-functionalized gold nanoparticles. Excitation wavelength was 420 nm for samples with porphyrin and 655 nm for samples with phthalocyanine.

Based on the fluorescence spectra, most of the attached porphyrinoids are quenched completely after attachment to gold nanoparticles and their fluorescence lifetime is too short to be fully resolved with the TCSPC method. Fluorescence lifetimes of porphyrin-functionalized gold nanoparticles were determined on a ps-timescale with the up-conversion measurements[IV] and the decay curves are shown Figure 4.12. The stretched-exponential model was applied for fitting the decays according to:[175-176]

$$F(t) = \exp\left[-\left(\frac{t}{\tau}\right)^{\beta}\right], \tag{4.4}$$

where τ is the fluorescence lifetime and β is the stretching parameter. The stretched-exponential model is applicable to heterogeneous systems. The stretching parameter describes the variation within the system: the smaller the value of β, the more diverse the system is. The choice of the fitting model is reasonable because all the porphyrins cannot be assumed to be attached in exactly a similar way to the particle surface.

The fluorescence intensity of *trans*-Por-AuNP decays faster than that of *cis*-Por-AuNP based on the lifetimes obtained from the stretched-exponential fit (Figure 4.12). Moreover, the stretching parameter is smaller for *trans*-Por-AuNP, which indicates a less uniform attachment of *trans*-Por compared to that of *cis*-Por. The fluorescence lifetime of a chromophore attached to a gold nanoparticle of certain size depends on the distance between the chromophore and the gold core, and on the orientation of the chromophore relative to the particle surface.[134] Previous studies on porphyrin-functionalized gold nanoparticles[124,139] and layered films of porphyrins and gold nanoparticles[II] have shown that the main mechanism for quenching of the porphyrin fluorescence is energy transfer. The linkers of the porphyrin molecules are short, ~1 nm. At this short distances, the energy transfer rate is highly dependent on the distance[133] and less dependent on the orientation of the chromophore[177]. When attached to gold nanoparticles, *cis*-Por can be expected to have a more perpendicular alignment relative to the particle surface based on the position of the linkers on the porphyrin core and the smaller mean molecular area. The *trans*-Por molecules can have a more parallel orientation relative to the particle surface, because the mean molecular area is higher than for *cis*-Por. In addition, the structure of *trans*-Por should allow a shorter distance between the particle surface and the porphyrin core. It is thus concluded that the main reason for the shorter fluorescence lifetime of *trans*-Por-AuNP compared to *cis*-Por-AuNP arises from the shorter distance between the porphyrin core and the particle surface.

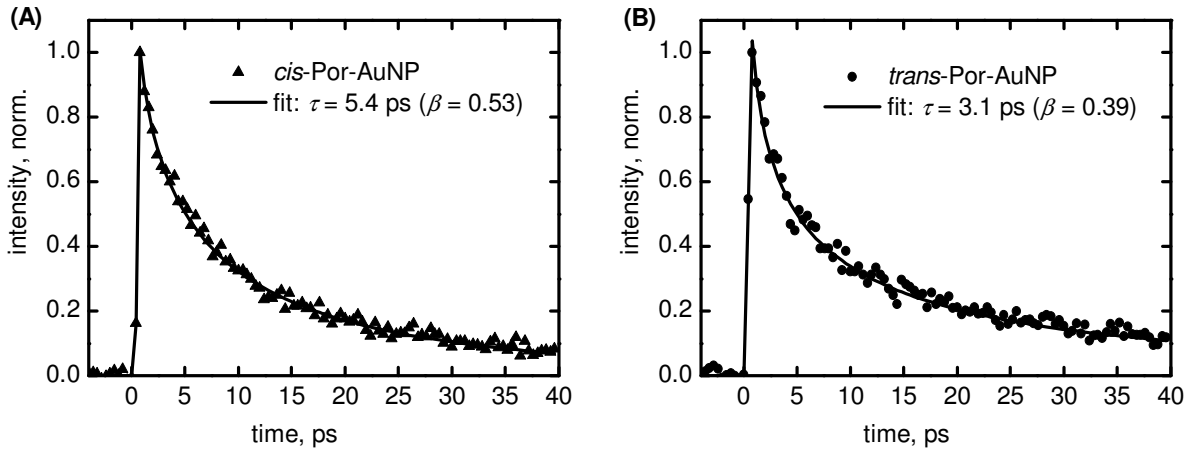

Figure 4.12. Fluorescence decay curves from up-conversion measurements for (A) *cis*-Por-AuNP and (B) *trans*-Por-AuNP. Excitation wavelength was 417 nm and monitoring wavelength 660 nm.

Selective excitation of the chromophore or the gold nanoparticle is not possible in porphyrin-functionalized gold nanoparticles, but this is not the case for phthalocyanine-functionalized gold nanoparticles. Transient absorption measurements with the pump-probe setup were done by exciting gold cores of Pc-AuNP at a wavelength of 500 nm. The decay component spectrum of TOABr-AuNP has two components (Figure 4.13A) arising from electron-phonon (3.4 ps) and phonon-phonon scattering (15 ps). The 3.4 ps component shows plasmon band bleaching around 540 nm, accompanied by photoinduced absorption at wavelengths of 590-710 nm. Pc-AuNP has only one component with a lifetime of 2.4 ps (Figure 4.13B). The Pc-AuNP spectrum shows the features from the gold nanoparticles, the plasmon bleaching at 530 nm and a photoinduced absorption at 575-645 nm. The bleaching of the plasmon band recovers faster in Pc-AuNP compared to TOABr-AuNP. Furthermore, there is a new feature at 645-730 nm that corresponds to bleaching of the phthalocyanine Q-band absorption. The phthalocyanines are not directly excited by the laser pulses, so they have to be excited by energy transfer from the gold cores, which correspondingly relax faster than in the TOABr-AuNP sample.

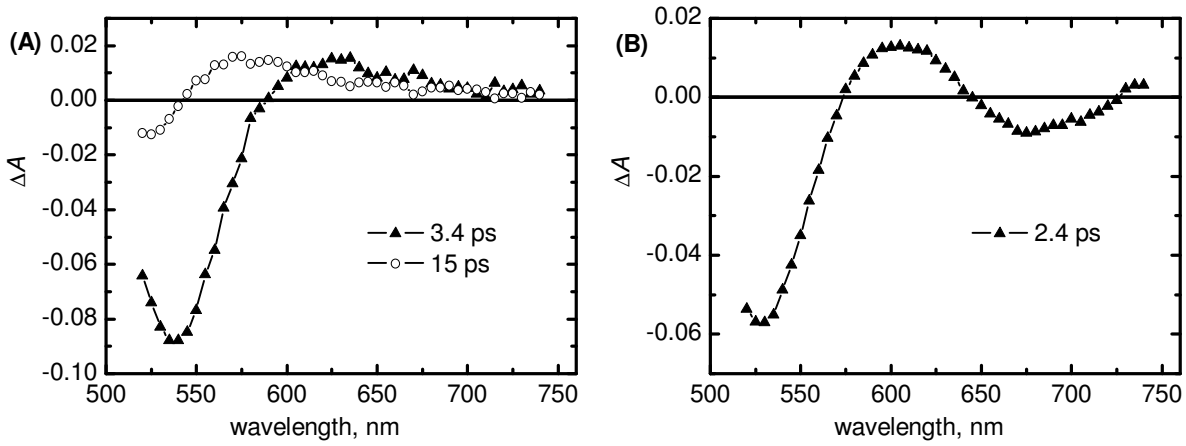

Figure 4.13. Decay component spectra obtained from global fitting of the pump-probe decay curves for (A) TOABr-AuNP in toluene and (B) Pc-AuNP in toluene. Excitation wavelength was 500 nm.

Phthalocyanines in Pc-AuNP cannot be excited selectively, but at 680 nm the phthalocyanines absorb more light than the gold cores. Pump-probe measurements using an excitation wavelength of 680 nm show that energy is transferred from the photoexcited phthalocyanines to the gold cores in Pc-AuNP, but along with energy transfer charge transfer is also observed.

4.2.2 Charge transfer in phthalocyanine-functionalized gold nanoparticles

Bleaching of the plasmon band at 530 nm is observed for TOABr-AuNP when excited at 680 nm (Figure 4.14A). The lifetime of the component corresponding to electron-phonon scattering is 1.8 ps. This feature was observed also after excitation at 500 nm. The phonon-phonon scattering is not observed after excitation at 680 nm, because the electronic temperature of the gold cores is not increased as much as after excitation at 500 nm. A component with a long lifetime, ~2.7 ns, is obtained for Pc in toluene solution (Figure 4.14A). The Pc component spectrum shows bleaching of the phthalocyanine Q-band around 700 nm and corresponds to the first excited singlet state of phthalocyanine. A toluene solution of Pc is not a good reference sample for Pc-AuNP, because in toluene the phthalocyanine molecules are dissolved well and no intermolecular interactions are observed. The phthalocyanine molecules in Pc-AuNP, however, have intermolecular interactions, as concluded from the absorption spectrum of Pc-AuNP solutions.

Three decay components are obtained for Pc-AuNP (Figure 4.14B). The ~2 ns component corresponds to those phthalocyanines that, even though attached to the particles, undergo no quenching of fluorescence and behave in a similar way as Pc in toluene. The 0.3 ps component observed for Pc-AuNP has the features of the first excited singlet state of phthalocyanine, and

additional photoinduced absorption at ~530 and 840-1000 nm. The 3.0 ps component for Pc-AuNP shows bleaching of the surface plasmon and phthalocyanine Q-band accompanied by a photoinduced absorption at 840-1000 nm. Recovery of the surface plasmon band is slower in Pc-AuNP compared with TOABr-AuNP, indicating energy transfer from phthalocyanines to the gold cores. Energy transfer from photoexcited attached chromophores has a similar effect as an increased excitation power: increased electronic temperature slows down the relaxation of the gold nanoparticles[178].

The phthalocyanine excited singlet state decays more rapidly in Pc-AuNP compared with TOABr-AuNP. This is partially explained by energy transfer to the gold cores but the appearance of the phthalocyanine radical cation absorption band[179-181] at 840-1000 nm for Pc-AuNP indicates electron transfer from the photoexcited phthalocyanines to the gold cores. The lifetime of the charge separated state is short, and fast charge recombination could arise from the short distance between the phthalocyanine and the gold nanoparticle. Electron transfer from photoexcited chromophores to gold nanoparticles has been observed to occur in pyrene-functionalized gold nanoparticles[108] and in electrostatic assemblies of chlorophyll and gold nanoparticles[107]. The HOMO level of metal-free phthalocyanine is 4.9 eV[182], and electron transfer from photoexcited phthalocyanine to gold nanoparticles is thus a valid mechanism for charge transfer in Pc-AuNP.

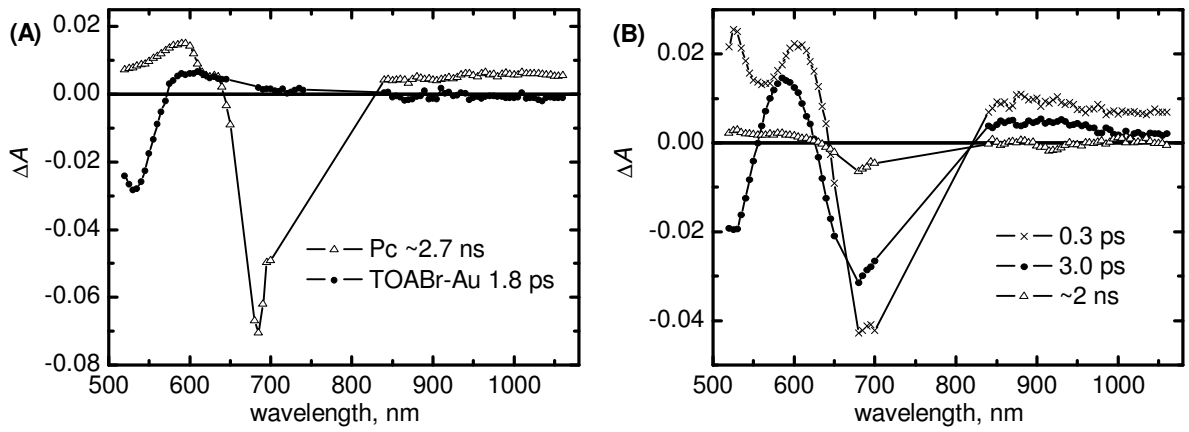

Figure 4.14. Decay component spectra obtained from global fitting of the pump-probe decay curves for (A) TOABr-AuNP and Pc in toluene and (B) Pc-AuNP in toluene. Excitation wavelength was 680 nm.

5 Conclusions

Controlled assembly of gold nanoparticles and chromophores into solid structures is necessary for building photoactive devices but the design of applications relies on knowledge of photoinduced processes within the gold nanoparticle-chromophore systems. The active role of the gold core in photoinduced charge transfer reactions in films was demonstrated by their capability of donating electrons to photoexcited porphyrins or fullerenes, and their capability for accepting electrons from photoexcited poly(hexylthiophene). Gold nanoparticle films act also as efficient energy acceptors in the case of porphyrin films. Both energy and charge transfer processes are known to take place in chromophore-gold nanoparticle systems and in the case of porphyrin-gold nanoparticle films the relative importances of these two processes could be estimated.

Films of porphyrin-fullerene dyads and gold nanoparticles are a step towards the construction of both structurally and functionally more complex systems. Porphyrin-fullerene dyads are known to undergo intramolecular photoinduced electron transfer via an exciplex intermediate state. Gold nanoparticles enhance charge transfer of the dyad film significantly when placed appropriately. In addition, the relaxation of the exciplex state of the dyad is affected by the adjacent gold nanoparticle film.

The thin film strategy followed was successful in organizing the particles and chromophores at close distances. The way to control even better their organization is to attach the chromophores, in this case porphyrins and phthalocyanines, directly to the metal core surface. Photoexcited porphyrins transfer energy very rapidly to the gold cores and energy transfer takes place also in phthalocyanine-functionalized gold nanoparticles. Selective excitation of the phthalocyanines leads also to electron transfer to the gold cores. Selective excitation of the gold cores in phthalocyanine-functionalized particles results in energy transfer to the phthalocyanines, demonstrating that the gold cores can behave as energy donors.

These conclusions show that although the photoinduced processes of gold nanoparticle-chromophore systems are generally known, they are strongly affected by the choice of the chromophore and by the design of the system. The next step in assembling chromophores and gold nanoparticles would be to organize functionalized gold nanoparticles into solid structures. These systems offer many possibilities for controlling organization and thus the rates of

photoinduced processes. Tunable parameters could include, for example, size and choice of the metal nanoparticle, choice of the chromophores, orientation and distance of the chromophore relative to the metal core and excitation energy. The gold nanoparticle-chromophore systems are a fragment of the booming area of nanotechnology that is and continues to develop, more and more as a part of everyday life and not just something from the pages of science fiction books.

References

1. M. Faraday, *Phil. Trans. R. Soc. Lond.* **1857**, *147*, 145.
2. P.P. Edwards, J.M. Thomas, *Angew. Chem. Int. Ed.* **2007**, *46*, 5480.
3. T.W. Odom, C.L. Nehl, *ACS Nano* **2008**, *2*, 612.
4. R. Sardar, A.M. Funston, P. Mulvaney, R.W. Murray, *Langmuir* **2009**, *in press*.
5. V. Amendola, M. Meneghetti, *Phys. Chem. Chem. Phys.* **2009**, *11*, 3805.
6. M. Pelton, J. Aizpurua, G. Bryant, *Laser & Photon. Rev.2* **2008**, *3*, 136.
7. P.K. Jain, X. Huang, I.H. El-Sayed, M.A. El-Sayed, *Acc. Chem. Res.* **2008**, *41*, 1578.
8. E. Hutter, J.H. Fendler, *Adv. Mater.* **2004**, *16*, 1685.
9. R.W. Murray, *Chem. Rev.* **2008**, *108*, 2688.
10. J. Ouyang, C.-W. Chu, D. Sieves, Y. Yang, *Appl. Phys. Lett.* **2005**, *86*, 123507.
11. L.D. Bozano, B.W. Kean, M. Beinhoff, K.R. Carter, P.M. Rice, J.C. Scott, *Adv. Funct. Mater.* **2005**, *15*, 1933.
12. W.L. Leong, P.S. Lee, S.G. Mhaisalkar, T.P. Chen, A. Dodabalapur, *Appl. Phys. Lett.* **2007**, *90*, 042906.
13. D.I. Gittins, D. Bethell, D.J. Schiffrin, R.J. Nichols, *Nature*, **2000**, *408*, 67.
14. M. Chen, D.W. Goodman, *Acc. Chem. Res.* **2006**, *39*, 739.
15. M.-C. Daniel, D. Astruc, *Chem. Rev.* **2004**, *104*, 293.
16. H. Haick, *J. Phys. Chem. D: Appl. Phys.* **2007**, *40*, 7173.
17. E. Katz, I. Willner, *Angew. Chem. Int. Ed.* **2004**, *43*, 6042.
18. V. Biju, T. Itoh, A. Anas, A. Sujith, M. Ishikawa, *Anal. Bioanal. Chem.* **2008**, *391*, 2469.
19. R. Shenhar, V.M. Rotello, *Acc. Chem. Res.* **2003**, *36*, 549.
20. Z. Shen, M. Yamada, M. Miyake, *J. Am. Chem. Soc.* **2007**, *129*, 14271.
21. S.I. Lim, C.-J. Zhong, *Acc. Chem. Res.* **2009**, *42*, 798.
22. M.E. El-Khouly, O. Ito, P.M. Smith, F. D'Souza, *J. Photochem. Photobiol. C* **2004**, *5*, 79.
23. D.M. Guldi, *Chem. Soc. Rev.* **2002**, *31*, 22.
24. H. Imahori, S. Fukuzumi, *Adv. Funct. Mater.* **2004**, *14*, 525.
25. K.G. Thomas, P.V. Kamat, *Acc. Chem. Res.* **2003**, *36*, 888.

26. J.R. Lakowicz, C.D. Geddes, I. Gryczynski, J. Malicka, Z. Gryczynski, K. Aslan, J. Lukomska, E. Matveeva, J. Zhang, R. Badugu, J. Huang, *J. Fluoresc.* **2004**, *14*, 425.
27. K. Aslan, S.N. Malyn, C.D. Geddes, *J. Fluoresc.* **2007**, *17*, 7.
28. O. Masala, R. Seshadri, *Annu. Rev. Mater. Res.* **2004**, *34*, 41.
29. D.I. Gittins, F. Caruso, *Ang. Chem. Int. Ed.* **2001**, *40*, 3001.
30. H. Hiramatsu, F.E. Osterloh, *Chem. Mater.* **2004**, *16*, 2509.
31. M. Aslam, L. Fu, M. Su, K. Vijayamohanan, V.P. Dravid, *J. Mater. Chem.* **2004**, *14*, 1795.
32. M. Schulz-Dobrick, K.V. Sarathy, M. Jansen, *J. Am. Chem. Soc.* **2005**, *127*, 12816.
33. F. Manea, C. Bindoli, S. Polizzi, L. Lay, P. Scrimin, *Langmuir*, **2008**, *24*, 4120.
34. M. Tréguer-Delapierre, J. Majimel, S. Mornet, E. Duguet, S. Ravaine, *Gold Bulletin* **2008**, *41*, 195.
35. B.V. Enüstün, J. Turkevich, *J. Am. Chem. Soc.* **1963**, *85*, 3317.
36. M. Brust, M. Walker, D. Bethell, D.J. Schiffrin, R. Whyman, *J. Chem. Soc., Chem. Commun.* **1994**, *7*, 801.
37. A.C. Templeton, W.P. Wuelfing, R.W. Murray, *Acc. Chem. Res.* **2000**, *33*, 27.
38. J. Fink, C.J. Kiely, D. Bethell, D.J. Schiffrin, *Chem. Mater.* **1998**, *10*, 922.
39. V.L. Jimenez, D.G. Georganopoulou, R.J. White, A.S. Harper, A.J. Mills, D. Lee, R.W. Murray, *Langmuir* **2004**, *20*, 6864.
40. J.M. Jørgensen, K. Erlacher, J.S. Pedersen, K.V. Gothelf, *Langmuir* **2005**, *21*, 10320.
41. M.J. Hostetler, J.E. Wingate,C.-J.Zhong, J.E. Harris,R.W. Vachet, M.R. Clark, J.D. Londono, S.J. Green, J.J. Stokes, G.D. Wignall, G.L. Glish, M.D. Porter, N.D. Evans, R.W. Murray, *Langmuir* **1998**, *14*, 17.
42. M.M. Maye, W. Zheng, F.L. Leibowitz, N.K. Ly, C.-J. Zhong, *Langmuir* **2000**, *16*, 490.
43. X.M. Lin, C.M. Sorensen, K.J. Klabunde, *J. Nanopart. Res.* **2000**, *2*, 157.
44. T. Shimizu, T. Teranishi, S. Hasegawa, M. Miyake, *J. Phys. Chem. B* **2003**, *107*, 2719.
45. T.G. Schaaff, M.N. Shafigullin, J.T. Khoury, I. Vezmar, R.L. Whetten, W.G. Cullen, P.N. First, C. Gutiérrez-Wing, J. Ascensio, M.J. Jose-Yacamán, *J. Phys. Chem. B* **1997**, *101*, 7885.
46. J.P. Wilcoxon, J.E. Martin, P. Provencio, *J. Chem. Phys.* **2001**, *115*, 998.
47. S. Link, M.A. El-Sayed, *Int. Rev. Phys. Chem.* **2000**, *19*, 409.
48. T.S. Ahmadi, S.L. Logunov, M.A. El-Sayed, *J. Phys. Chem.* **1996**, *100*, 8053.
49. K.L. Kelly, E. Coronado, L.L. Zhao, G.C. Schatz , *J. Phys. Chem. B* **2003**, *107*, 668.
50. P. K. Jain, K. S. Lee, I.H. El-Sayed, M.A. El-Sayed, *J. Phys. Chem. B* **2006**, *110*, 7238.

51. X. Liu, M. Atwater, J. Wang, Q. Huo, *Colloids & Surfaces B: Biointerfaces* **2007**, *58*, 3.
52. M.M. Alvarez, J.T. Khoury, T.G. Schaaff, M.N. Shafigullin, I. Vezmar, R.L. Whetten, *J. Phys. Chem. B* **1997**, *101*, 3706.
53. C.P. Vinod, G.U. Kulkarni, C.N.R. Rao, *Chem. Phys. Lett.* **1998**, *289*, 329.
54. S. Link, C. Burda, Z.L. Wang, M.A. El-Sayed, *J. Chem. Phys.* **1999**, *111*, 1255.
55. C. Voisin, N. Del Fatti, D. Christofilos, F. Vallée, *J. Phys. Chem. B* **2001**, *105*, 2264.
56. M. Perner, P. Bost, U. Lemmer, G. von Plessen, J. Feldmann, U. Becker, M. Mennig, M. Schmitt, H. Schmidt, *Phys. Rev. Lett.* **1997**, *78*, 2192.
57. S.L. Logunov, T.S. Ahmadi, M.A. El-Sayed, J.T. Khoury, R.L. Whetten, *J. Phys. Chem. B* **1997**, *101*, 3713.
58. J.H. Hodak, I. Martini, G.V. Hartland, *J. Phys. Chem. B* **1998**, *102*, 6958.
59. M.B. Mohamed, T.S. Ahmadi, S. Link, M. Braun, M.:A El-Sayed, *Chem. Phys. Lett.* **2001**, *343*, 55.
60. J.P. Wilcoxon, J.E. Martin, F. Parsapour, B. Wiedenman, D.F. Kelley, *J. Chem. Phys.* **1998**, *108*, 9137.
61. T. Huang, R.W. Murray, *J. Phys. Chem. B* **2001**, *105*, 12498.
62. S. Link, A. Beeby, S. FitzGerald, M. A. El-Sayed, T.G. Schaaff, R.L. Whetten, *J. Phys. Chem. B* **2002**, *106*, 3410.
63. T.P. Bigioni, R.L. Whetten, Ö. Dag, *J. Phys. Chem. B* **2000**, *104*, 6983.
64. Y. Yang, S. Chen, *Nano Lett.* **2003**, *3*, 75.
65. G. Wang, R. Guo, G. Kalyuzhny, J.-P. Choi, R.W. Murray, *J. Phys. Chem. B* **2006**, *110*, 20282.
66. J. Zheng, J.T. Petty, R.M. Dickson, *J. Am. Chem. Soc.* **2003**, *125*, 7780.
67. G. Hodes, *Adv. Mater.* **2007**, *19*, 639.
68. O.P. Varnavski, T. Goodson III, M.B. Mohamed, M.A. El-Sayed, *Phys. Rev. B* **2005**, *72*, 235405.
69. Y.-N. Hwang, D.H. Jeong, H.J. Shin, D. Kim, S.C. Jeoung, S.H. Han, J.-S. Lee, G. Cho, *J. Phys. Chem. B* **2002**, *106*, 7581.
70. E. Dulkeith, T. Niederreichholz, T.A. Klar, J. Feldmann, G. von Plessen, D.I. Gittins, K.S. Mayya, F. Caruso, *Phys. Rev. B* **2004**, *70*, 205424.
71. S. Chen, R.S. Ingram, M.J. Hostetler, J.J. Pietron, R.W. Murray, T.G. Schaaf, J.T. Khoury, M.M. Alvarez, R.L. Whetten, *Science* **1998**, *280*, 2098.
72. N.K. Chaki, P. Singh, C.V. Dharmadhikari, K.P. Vijayamohanan, *Langmuir* **2004**, *20*, 10208.

73. R.S. Ingram, M.J. Hostetler, R.W. Murray, T.G. Schaaff, J.T. Khoury, R.L. Whetten, T.G. Bigioni, D.K. Guthrie, P.N. First, *J. Am. Chem. Soc.* **1997**, *119*, 9279.

74. B.M. Quinn, P. Liljeroth, V. Ruiz, T. Laaksonen, K. Kontturi, *J. Am. Chem. Soc.* **2003**, *125*, 6644.

75. J.J. Pietron, J.F. Hicks, R.W. Murray, *J. Am. Chem. Soc.* **1999**, *121*, 5565.

76. W.P. Wuelfing, S.J. Green, J.J. Pietron, D.E. Cliffel, R.W. Murray, *J. Am. Chem. Soc.* **2000**, *122*, 11465.

77. R.H. Terrill, T.A. Postlethwaite, C. Chen, C.-D. Poon, A. Terzis, A. Chen, J.E. Hutchison, M.R. Clark, G. Wignall, J.D. Londono, R. Superfine, M. Falvo, C.S. Johnson Jr., E.T. Samulski, R.W. Murray, *J. Am. Chem. Soc.* **1995**, *117*, 12537.

78. S. Chen, *Anal. Chim. Acta* **2003**, *496*, 29.

79. P. Liljeroth, D. Vanmaekelbergh, V. Ruiz, K. Kontturi, H. Jiang, E. Kauppinen, B.M. Quinn, *J. Am. Chem. Soc.* **2004**, *126*, 7126.

80. N. Kobayashi, T. Fukuda: *Recent progress in phthalocyanine chemistry: Synthesis and characterization*, in S.H. Kim (Ed.): *Functional dyes*, Elsevier, **2006**.

81. P.-C. Lo, X. Leng, D.K.P. Ng, *Coord. Chem. Rev.* **2007**, *251*, 2334.

82. C.M. Drain, A. Varotto, I. Radivojevic, *Chem. Rev.* **2009**, *109*, 1630.

83. H.W. Kroto, J.R. Heath, S.C. O'Brien, R.F. Curland, R.E. Smalley, *Nature* **1985**, *318*, 162.

84. M.S. Mauter, M. Elimelech, *Environ. Sci. Technol.* **2008**, *42*, 5843.

85. Q. Xie, E. Pérez-Cordero, L. Echegoyen, *J. Am. Chem. Soc.* **1992**, *114*, 3978.

86. D. Kuciauskas, S. Lin, G.R. Seely, A.L. Moore, T.A. Moore, D. Gust, T. Drovetskaya, C.A. Reed, P.D.W. Boyd, *J. Phys. Chem. B* **1996**, *100*, 15926.

87. H. Imahori, K. Hagiwara, M. Aoki, T. Akiyama, S. Taniguchi, T. Okada, M. Shirakawa, Y. Sakata, *J. Am. Chem. Soc.* **1996**, *118*, 11771.

88. N. Armaroli, G. Marconi, L. Echegoyen, J.-P. Bourgeois, F. Diederich, *Chem. Eur. J.* **2000**, *6*, 1629.

89. F. D'Souza, G.R. Deviprasad, M.E. El-Khouly, M. Fujitsuka, O. Ito, *J. Am. Chem. Soc.* **2001**, *123*, 5277.

90. T.J. Kesti, N.V. Tkachenko, V. Vehmanen, H. Yamada, H. Imahori, S. Fukuzumi, H. Lemmetyinen, *J. Am. Chem. Soc.* **2002**, *124*, 8067.

91. H. Yamada, H. Imahori, Y. Nishimura, I. Yamazaki, T.K. Ahn, S.K. Kim, D. Kim, S. Fukuzumi, *J. Am. Chem. Soc.* **2003**, *125*, 9129.

92. V. Chukharev, T. Vuorinen, A. Efimov, N.V. Tkachenko, *Langmuir* **2005**, *21*, 6385.

93. E. Dietel, A. Hirsch, E. Eichhorn, A. Rieker, S. Hackbarth, B. Roder, *Chem. Commun.* **1998**, 1981.

94. V. Chukharev, N.V. Tkachenko, A. Efimov, D.M. Guldi, A. Hirsch, M. Scheloske, H. Lemmetyinen, *J. Phys. Chem. B* **2004**, *108*, 16377.

95. D.I. Schuster, P. Cheng, P.D. Jarowski, D.M. Guldi, C. Luo, L. Echegoyen, S. Pyo, A.R. Holzwarth, S.E. Braslavsky, R.M. Williams, G. Klihm, *J. Am. Chem. Soc.* **2004**, *126*, 7257.

96. O. Stenzel, A. Stendal, K. Voigtsberger, C. von Borzyskowski, *Solar Energy Mater. Solar Cells* **1995**, *37*, 337.

97. M. Westphalen, U. Kreibig, J. Rostalski, H. Lüth, D. Meissner, *Solar Energy Mater. Solar Cells* **2000**, *61*, 97.

98. Y. Tian, T. Tatsuma, *J. Am. Chem. Soc.* **2005**, *127*, 7632.

99. Z.H. Chen, Y.B. Tang, C.P. Liu, Y.H. Leung, G.D. Yuan, L.M. Chen, Y.Q. Wang, I. Bello, J.A. Zapien, W.J. Zhang, C.S. Lee, S.T. Lee, *J. Phys. Chem. C* **2009**, *113*, 13433.

100. A. Yakimov, S.R. Forrest, *Appl. Phys. Lett.* **2002**, *80*, 1667.

101. Y. Sato, K. Yamagishi, M. Yamashita, *Opt. Rev.* **2005**, *12*, 324.

102. Y.H. Su, W.H. Lai, L.G. Teoh, M.H. Hon, J.L. Huang, *Appl. Phys. A* **2007**, *88*, 173.

103. S.W. Tong, C.F. Zhang, C.Y. Jiang, G. Liu, Q.D. Ling, E.T. Kang, D.S.H. Chan, C. Zhu, *Chem. Phys. Lett.* **2008**, *453*, 73.

104. K. Kim, D.L. Carroll, *Appl. Phys. Lett.* **2005**, *87*, 203113.

105. T. Huang, R.W. Murray, *Langmuir* **2002**, *18*, 7077.

106. C. Fan, S. Wang, J.W. Hong, G.C. Bazan, K.W. Plaxco, A.J. Heeger, *Proceedings of the National Academy of Sciences of the USA* **2003**, *100*, 6297.

107. S. Barazzouk, P. V. Kamat, S. Hotchandani, *J. Phys. Chem. B* **2005**, *109*, 716.

108. B.I. Ipe, K. G. Thomas, S. Barazzouk, S. Hotchandani, P.V. Kamat, *J. Phys. Chem. B* **2002**, *106*, 18.

109. A. Aguila, R.W. Murray, *Langmuir* **2000**, *16*, 5949.

110. T. Gu, J.K. Whitesell, M.A. Fox, *Chem. Mater.* **2003**, *15*, 1358.

111. T.L. Jennings, M.P. Singh, G.F. Strouse, *J. Am. Chem. Soc.* **2006**, *128*, 5462.

112. T. Sen, S. Sadhu, A. Patra, *Appl. Phys. Lett.* **2007**, *91*, 043104.

113. M.P. Rowe, K.E. Plass, K. Kim, C. Kurdak, E.T. Zellers, A.J. Matzger, *Chem. Mater.* **2004**, *16*, 3513.

114. M.J. Hostetler, S.J. Green, J.J. Stokes, R.W. Murray, *J. Am. Chem. Soc.* **1996**, *118*, 4212.

115. H. Choo, E. Cutler, Y.-S. Shon, *Langmuir* **2003**, *19*, 8555.
116. N. Nerambourg, M.H.V. Werts, M. Charlot, M. Blanchard-Desce, *Langmuir* **2007**, *23*, 5563.
117. A.C. Templeton, M.J. Hostetler, E.K. Warmoth, S. Chen, C.M. Hatshorn, V.M. Krishnamurthy, M.D.E. Forbes, R.W. Murray, *J. Am. Chem. Soc.* **1998**, *120*, 4845.
118. Y.-S. Shon, H. Choo, *C.R. Chimie* **2003**, *6*, 1009.
119. A.R. Tao, J. Huang, P. Yang, *Acc. Chem. Res.* **2008**, *41*, 1662.
120. F. Caruso, *Adv. Mater.* **2001**, *13*, 11.
121. V. Kriegisch, C. Lambert, *Top. Curr. Chem.* **2005**, *258*, 257.
122. B.I. Ipe, K.G. Thomas, *J. Phys. Chem. B* **2004**, *108*, 13265.
123. T. Pons, I.L. Medintz, K.E. Sapsford, S. Higashiya, A.F. Grimes, D.S. English, H. Mattoussi, *Nano Lett.* **2007**, *7*, 3157.
124. H. Imahori, M. Arimura, T. Hanada, Y. Nishimura, I. Yamazaki, Y. Sakata, S. Fukuzumi, *J. Am. Chem. Soc.* **2001**, *123*, 335.
125. P.K. Sudeep, B.I. Ipe, K.G. Thomas, M.V. George, S. Barazzouk, S. Hotchandani, P.V. Kamat, *Nano Lett.* **2002**, *2*, 29.
126. B. Valeur: *Molecular Fluorescence Principles and Applications*, Wiley-VCH, Federal Republic of Germany, **2002**.
127. H. Kuhn, *J. Chem. Phys.* **1970**, *53*, 101.
128. J. Hill, S.Y. Heriot, O. Worsfold, T.H. Richardson, A.M. Fox, D.D.C. Bradley, *Phys. Rev. B* **2004**, *69*, 041303.
129. C.S. Yun, A. Javier, T. Jennings, M. Fisher, S. Hira, S. Peterson, B. Hopkins, N.O. Reich, G.F. Strouse, *J. Am. Chem. Soc.* **2005**, *127*, 3115.
130. T. Sen, A. Patra, *J. Phys. Chem. C* **2008**, *112*, 3216.
131. E. Dulkeith, A.C. Morteani, T. Niederreichholz, T.A. Klar, J. Feldmann, S.A. Levi, F.C.J.M. van Veggel, D.N. Reinhoudt, M. Möller, D.I. Gittins, *Phys. Rev. Lett.* **2002**, *89*, 203002.
132. E. Dulkeith, M. Ringler, T.A. Klar, J. Feldmann, A.M. Javier, W.J. Parak, *Nano Lett.* **2005**, *5*, 585.
133. S. Vukovic, S. Corni, B. Mennucci, *J. Phys. Chem. C* **2009**, *113*, 121.
134. J. Gersten, A. Nitzan, *J. Chem. Phys.* **1981**, *75*, 1139.
135. J.R. Lakowicz, *Anal. Biochem.* **2005**, *337*, 171.
136. S. Yamada, T. Tasaki, T. Akiyama, N. Terasaki, S. Nitahara, *Thin Solid Films* **2003**, *438-439*, 70.

137. S. Fukuzumi, Y. Endo, Y. Kashiwagi, Y. Araki, O. Ito, H. Imahori, *J. Phys. Chem. B* **2003**, *107*, 11979.
138. P.D. Beer, D.P. Cormode, J.J. Davis, *Chem. Commun.* **2004**, 414.
139. H. Imahori, Y. Kashiwagi, Y. Endo, T. Hanada, Y. Nishimura, I. Yamazaki, Y. Araki, O. Ito, S. Fukuzumi, *Langmuir* **2004**, *20*, 73.
140. T. Hasobe, H. Imahori, P.V. Kamat, T.K. Ahn, S.K. Kim, D. Kim, A. Fujimoto, T. Hirakawa, S. Fukuzumi, *J. Am. Chem. Soc.* **2005**, *127*, 1216.
141. H. Imahori, A. Fujimoto, S. Kang, H. Hotta, K. Yoshida, T. Umeyama, Y. Matano, S. Isoda, M. Isosomppi, N.V. Tkachenko, H. Lemmetyinen, *Chem. Eur. J.* **2005**, *11*, 7265.
142. M. Kanehara, H. Takahashi, T. Teranishi, *Angew. Chem. Int. Ed.* **2008**, *47*, 307.
143. D.C. Hone, P.I. Walker, R. Evans-Gowing, S. FitzGerald, A. Beeby, I. Chambrier, M.J. Cook, D.A. Russell, *Langmuir* **2002**, *18*, 2985.
144. M.E. Wieder, D.C. Hone, M.J. Cook, M.M. Handsley, J. Gavrilovic, D.A. Russell, *Photochem. Photobiol. Sci.* **2006**, *5*, 727.
145. T. Akiyama, M. Nakada, N. Terasaki, S. Yamada, *Chem. Commun.* **2006**, 395.
146. K. Sugawa, T. Akiyama, H. Kawazumi, S. Yamada, *Langmuir* **2009**, *25*, 3887.
147. M. Brust, C.J. Kiely, D. Bethell, D.J. Schiffrin, *J. Am. Chem. Soc.* **1998**, *120*, 12367.
148. F. Deng, Y. Yang, S. Hwang, Y.-S. Shon, S. Chen, *Anal. Chem.* **2004**, *76*, 6102.
149. V. Amendola, G. Mattei, C. Cusan, M. Prato, M. Meneghetti, *Synth. Met.* **2005**, *155*, 283.
150. A. Efimov, P. Vainiotalo, N.V. Tkachenko, H. Lemmetyinen, *J. Porphyrins Phthalocyanines* **2003**, *7*, 610.
151. X. Camps, A. Hirsch, *J. Chem. Soc., Perkin Trans. 1* **1997**, 1595.
152. T. Vuorinen, K. Kaunisto, N.V. Tkachenko, A. Efimov, H. Lemmetyinen, *Langmuir* **2005**, *21*, 5383.
153. D.V. Leff, P.C. Ohara, J.R. Heath, W.M. Gelbart, *J. Phys. Chem.* **1995**, *99*, 7036.
154. R.L. Whetten, J.T. Khoury, M.M. Alvarez, S. Murthy, I. Vezmar, Z.L. Wang, P.W. Stephens, C.L. Cleveland, W.D. Luedtke, U. Landman, *Adv. Mater.* **1996**, *8*, 428.
155. J.M. Tour, L. Jones II, D.L. Pearson, J.J.S. Lamba, T.P. Burgin, G.M. Whitesides, D.L. Allara, A.N. Parikh, S.V. Atre, *J. Am. Chem. Soc.* **1995**, *117*, 9529.
156. E.Sariola, A. Kotiaho, N.V. Tkachenko, H. Lemmetyinen, A. Efimov, *J. Porphyrins Phthalocyanines*, accepted for publication.
157. G.G. Roberts, *Adv. Phys.* **1985**, *34*, 475.

158. G.T. Barnes, I.R. Gentle: *Interfacial Science*, Oxford University Press, Great Britain, **2005**.

159. N.V. Tkachenko: *Optical Spectroscopy Methods and Instrumentations*, Elsevier, Amsterdam, **2006**.

160. M. Ikonen, A. Sharonov, N.V. Tkachenko, H. Lemmetyinen, *Adv. Mater. Opt. Electron.* **1993**, *2*, 115.

161. N.V. Tkachenko, P.H. Hynninen, H. Lemmetyinen, *Chem. Phys. Lett.* **1996**, *261*, 234.

162. N.V. Tkachenko, E. Vuorimaa, T. Kesti, A.S. Alekseev, A.Y. Tauber, P.H. Hynninen, H. Lemmetyinen *J. Phys. Chem. B* **2000**, *104*, 6371.

163. P.J. Goodhew, F.J. Humphreys, R. Beanland: *Electron Microscopy and Analysis*, Taylor & Francis Ltd., **2000**. Online version available at http://site.ebrary.com.

164. H.J. Moore, N. Spencer (Ed.): *Encyclopedia of Chemical Physics and Physical Chemistry, Vol. 2 Methods*, CRC Press, **2001**. Online version available at http://www.physicsnetbase.com

165. S. Hénon, J. Meunier, *Rev. Sci. Instrum.* **1991**, *62*, 936.

166. T. Kaercher, D. Hönig, D. Möbius, *Int. Ophthalmol.* **1993**, *17*, 341.

167. Y. Sun, A.I. Frenkel, H. White, L. Zhang, Y. Zhu, H. Xu, J.C. Yang, T. Koga, V. Zaitsev, M.H. Rafailovich, J.C. Sokolov, *J. Phys. Chem. B* **2006**, *110*, 23022.

168. J.R. Heath, C.M. Knobler, D.V. Leff, *J. Phys. Chem. B* **1997**, *101*, 189.

169. D.R. Lide (Ed.): *CRC Handbook of Chemistry and Physics*, 89th ed., CRC Press, **2009**. Online version available at http://www.hbcpnetbase.com

170. K. Takahashi, Y. Takano, T. Yamaguchi, J. Nakamura, C. Yokoe, K. Murata, *Synth. Met.* **2005**, *155*, 51.

171. J.-J. Yun, H.-S. Jung, S.-H. Kim, E.-M. Han, V. Vaithianathan, S.A. Jenekhe, *Appl. Phys. Lett.* **2005**, *87*, 123102.

172. H. Ishii, A. Seko, A. Kawakami, K. Umishita, Y. Ouchi, K. Seki, *Mater. Res. Soc. Symp. Proc.* **2003**, *771*, L3.5.1.

173. H. Lehtivuori, A. Efimov, H. Lemmetyinen, N.V. Tkachenko, *Chem. Phys. Lett.* **2007**, *437*, 238.

174. W.J. Schutte, M. Sluyters-Rebbach, J.H. Sluyters, *J. Phys. Chem.* **1993**, *97*, 6069.

175. M.N. Berberan-Santos, E.N. Bodunov, B. Valeur, *Chem. Phys.* **2005**, *315*, 171.

176. R. Metivier, I. Leray, J.-P. Lefevre, M. Roy-Auberger, N. Zanier-Szydlowski, B. Valeur, *Phys. Chem. Chem. Phys.* **2003**, *5*, 758.

177. S. Bhowmick, S. Saini, V.B. Shenoy, B. Bagchi, *J. Chem. Phys.* **2006**, *125*, 181102.

178. T. Gu, T. Ye, J.D. Simon, J.K. Whitesell, M.A. Fox, *J. Phys. Chem. B* **2003**, *107*, 1765.

179. C. Farren, C.A. Christensen, S. FitzGerald, M.R. Bryce, A. Beeby, *J. Org. Chem.* **2002**, *67*, 9130.

180. E. Ough, Z. Gasyna, M.J. Stillman, *Inorg. Chem.* **1991**, *30*, 2301.

181. T. Nojiri, M.M. Alam, H. Konami, A. Watanabe, O. Ito, *J. Phys. Chem. A* **1997**, *101*, 7943.

182. Y. Terao, H. Sasabe, C. Adachi, *Appl. Phys. Lett.* **2007**, *90*, 103515.